Environmental Science: Atmospheres

ROYAL SOCIETY OF CHEMISTRY

CRITICAL REVIEW

View Article Online
View Journal | View Issue

Check for updates

Cite this: *Environ. Sci.: Atmos.*, 2022, **2**, 111

Particulate nitrate photolysis in the atmosphere

Masao Gen, [a] Zhancong Liang, [bc] Ruifeng Zhang, [bc] Brix Raphael Go [bc] and Chak K. Chan *[bcd]

Multiphase and heterogeneous photochemistry is an emerging component of atmospheric and air pollution research. It is primarily driven by reactions of photochemically produced free radicals in the particle phase with dissolved gaseous species. It has significant implications to promote the oxidation of aerosol particles, one of the most important atmospheric processes for secondary inorganic and organic aerosol formation. Nitrate is an increasingly important component in atmospheric aerosol particles with the trend of dominating over sulfate. Nitrate photolysis has long been known to produce highly reactive oxidants such as hydroxyl radicals in both gas and bulk or cloud phases. Recent studies have found that nitrate photolysis in the particle phase (*i.e.*, particulate nitrate photolysis) proceeds faster than bulk solutions or cloud droplets by many orders of magnitude. Factors and mechanisms affecting particulate nitrate photolysis include the formation of solvent cages, pH, and co-existing species, but they remain controversial. Hence, the impact of nitrate photolysis in atmospheric chemistry is still uncertain. This paper reviews the current status of knowledge about the effects of particulate nitrate photolysis, instead of relatively well-known gas- and bulk-phase nitrate photolysis, in the atmosphere. Recommendations for future research directions on the mechanistic understanding of particulate nitrate photolysis and its parameterizations in air quality models are also made.

Received 26th October 2021
Accepted 12th January 2022

DOI: 10.1039/d1ea00087j

rsc.li/esatmospheres

Open Access Article. Published on 13 de gener 2022. Downloaded on 2/2/2026 23:46:41.
This article is licensed under a Creative Commons Attribution 3.0 Unported Licence.

Environmental significance

Atmospheric particulate matter or aerosol particles, directly and indirectly, impact climate, regional air quality, and human health. The atmosphere is a giant and strongly oxidizing chemical reactor, and the atmospheric oxidizing capacity is closely associated with the chemical evolution of aerosol particles. Inorganic nitrate photolysis can contribute to the atmospheric oxidizing capacity by generating strong oxidants such as hydroxyl radical. Nitrate photolysis in aerosol particles is accelerated by many orders of magnitude relative to bulk solution reactions, but factors and mechanisms affecting particulate nitrate photolysis remain controversial. As a result, the impact of particulate nitrate photolysis on the atmospheric oxidizing capacity is still uncertain. We review the current status of knowledge about particulate nitrate photolysis in the atmosphere.

1. Introduction

Atmospheric particulate matter (PM) or aerosol particles have significant impacts on climate, regional air quality, and human health.[1] PM is emitted from many diverse anthropogenic and biogenic sources.[2] During its atmospheric lifetime (~a week), PM is subjected to many processes leading to physical and chemical transformations such as changes in its size, morphology, and chemical composition.[3] The Earth's atmosphere is a giant and strongly oxidizing chemical reactor, and hence the atmospheric oxidizing capacity is closely associated with the evolution of PM's composition and properties. Despite the crucial importance of PM in the atmospheric environment, our understanding of the physical and chemical transformation of PM is far from complete. In this paper, we will use the terms PM and aerosol particles interchangeably.

Sunlight, especially in the ultraviolet spectral region, is a source of atmospheric free radicals that drive the chemical changes in the atmosphere.[2] The sunlight reaching low altitudes has a wavelength longer than 290 nm.[4] One of the essential atmospheric photochemical processes is the generation of free radicals through gas-phase photochemistry.[5,6] The gas-phase reactions are crucial in ozone depletion in the stratosphere and tropospheric oxidant production and organic oxidation, relevant to the abundance of climate forcing agents.[7] However, the chemistry occurring within or on aerosol particles and cloud droplets is much less known. In this paper, we will focus on the photochemical processes of PM or aerosol particles. Solar radiation gives the energy to initiate photochemical reactions of aerosol particles and gaseous species. Multiphase and heterogenous photochemistry is an emerging field in

[a]*Faculty of Frontier Engineering, Institute of Science and Engineering, Kanazawa University, Kanazawa, 920-1192, Japan*
[b]*School of Energy and Environment, City University of Hong Kong, Hong Kong, China. E-mail: chak.k.chan@cityu.edu.hk*
[c]*City University of Hong Kong Shenzhen Research Institute, Shenzhen, China*
[d]*Guy Carpenter Asia-Pacific Climate Impact Center, City University of Hong Kong, Hong Kong, China*

© 2022 The Author(s). Published by the Royal Society of Chemistry

Open Access Article. Published on 13 de gener 2022. Downloaded on 2/2/2026 23:46:41.
This article is licensed under a Creative Commons Attribution 3.0 Unported Licence.

atmospheric and air pollution research, and it has the potential to promote atmospheric oxidation greatly.[8]

The importance of multiphase and heterogeneous photochemistry in the atmosphere has been demonstrated in many laboratory studies. For example, multiphase photolysis of aerosols containing a trace amount of photosensitive compounds (*e.g.*, humic acid) produces strong oxidants (*e.g.*, superoxide, hydroxyl, nitrate, and organic radicals) in the particle phase.[9] These in-particle oxidants can lead to fast uptake of non-condensable volatile organic compounds (VOCs) of limonene and isoprene without gas-phase oxidation. That study challenges the traditional view that such non-condensable VOCs need to be oxidized in the gas phase before partitioning into the particle phase to form secondary organic aerosol.[3,10] Another example is the reactive uptake of sulfur dioxide (SO_2) by irradiated particulate nitrate. Nitrate photolysis can produce in-particle hydroxyl (OH), nitrogen dioxide (NO_2) radicals, and nitrite, promoting the oxidation of dissolved SO_2 in the particle phase for sulfate production.[11,12] This photochemistry can potentially reconcile the difference between field measurements and model estimations of sulfate formation during highly polluted episodes in China.[13] Thus, multiphase and heterogenous photochemistry has significant implications in atmospheric chemistry.

Among the photolytic sources of strong oxidants such as irradiated mineral dust,[14,15] iron–organic complexes,[16,17] nitrate/nitrite,[18,19] hydrogen peroxide,[20] and hypochlorous acid,[21,22] inorganic nitrate anion (NO_3^-) is an increasingly important component in atmospheric aerosol particles as sulfate concentrations decrease. Sulfate was the dominant inorganic constituent in atmospheric aerosol particles and is mainly formed from SO_2 oxidation. SO_2 emission has reduced globally while there is a modest increase in ammonia emission due to intensified agricultural activity livestock farming following population growth.[23] For instance, SO_2 emissions in China have decreased by 75% since 2007, while India is surpassing China as the world's largest emitter of anthropogenic SO_2.[24] Across the United States, SO_2 emissions have decreased at ~6% per year from 2001 to 2010.[25] This SO_2 reduction elevates aerosol pH and facilitates nitrate partitioning into the aerosol phase, leading to the growing nitrate dominance over sulfate. Nitrate-dominated aerosols have been observed in many locations, including the USA,[26] Europe,[27,28] and East Asia.[29–32]

Inorganic nitrate photolysis[18,33] has an influence on NO_x, OH, and O_3 mass burdens in the atmosphere.[34] It can be also used as a photolytic source of OH radicals to remove hazardous organic pollutants in environmental waters in advanced oxidation technologies.[35,36] The mechanism of nitrate photolysis has been extensively studied in bulk solutions,[18,33] but that of particulate nitrate photochemistry is not fully assessed despite increasing evidence of the nitrate-dominated aerosols as mentioned above. When nitrate photolysis is confined in a small droplet or a deliquesced aerosol particle, which is referred to as particulate nitrate photolysis in this review, it is accelerated by order(s) of magnitude relative to bulk solution reactions.[11,37–40] Several factors/mechanisms affecting particulate nitrate photolysis such as solvent cages,[41] pH,[42] and co-existing species[43] have been suggested in the literature, but they remain controversial. As a result, the impact of nitrate photolysis in atmospheric chemistry is still uncertain. Similarly, organic nitrates play important roles in the atmosphere because their fate including photolysis could affect the NO_x recycling and O_3 production.[44,45] Photolysis of organic nitrates can produce NO_2 and HO_2,[46] which may have impacts on subsequent reactions in the particle phase.[47] However, there are very few studies on photolysis of particulate organic nitrates, and thus we limit our focus to that of particulate inorganic nitrate.

This paper reviews the current status of knowledge about the effects of particulate inorganic nitrate photolysis, instead of relatively well-known gas- and bulk-phase nitrate photolysis, in the atmosphere. We begin with an overview of nitrate photolysis mechanisms, followed by discussing factors affecting the product yields of particulate nitrate photolysis. We then review the quantum yields and nitrate photolysis rate constants reported in the literature for quantifying the impacts of nitrate photolysis in the atmosphere and used in air quality models. Finally, we summarize chemical reactions related to nitrate photolysis in the particle phase. Particulate nitrate photolysis generates gas-phase oxidants such as NO_2 and HONO, which can tremendously affect ozone and halogen chemistry.[34] However, the gas-phase reactions are not addressed in this review. Critical issues and recommendations for future research directions will be presented at the end of this review paper.

2. Nitrate photolysis mechanism

Nitrate anion (NO_3^-) is a crucial chromophore in environmental waters. Nitrate can be photolyzed in both aqueous[48] and crystalline states.[49] In this section, we briefly review nitrate photolysis mechanisms relevant to the atmosphere. For more detailed mechanisms of nitrate photolysis, we refer readers to the previous reviews.[18,33]

As a result of the absorption of UV photons, electrons of nitrate anions can move from their ground state to an unoccupied or partially occupied molecular orbital of higher energy. Because the energy level of UV light is of the same order as the enthalpies of the covalent bonds, this additional energy results in a bond cleavage, which splits the excited nitrate, $[NO_3^-]^*$, into two fragments, a process known as photolysis (R1). Nitrate photolysis produces oxidants such as hydroxyl (OH) and nitrogen dioxide

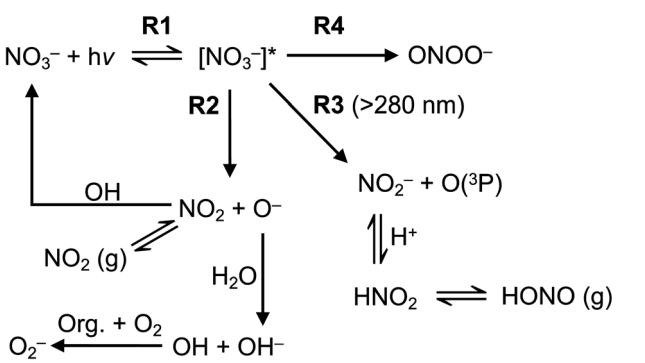

Fig. 1 Simplified nitrate photolysis mechanisms.[50]

© 2022 The Author(s). Published by the Royal Society of Chemistry

Open Access Article. Published on 13 de gener 2022. Downloaded on 2/2/2026 23:46:41.
This article is licensed under a Creative Commons Attribution 3.0 Unported Licence.

(NO_2) radicals and nitrite ions (NO_2^-) ((R2) and (R3); Fig. 1).[50] Furthermore, $[NO_3^-]^*$ can isomerize (R4). These photoproducts can have potentially significant impacts on subsequent reactions in aerosol particles, as will be discussed in Section 5. The absorption spectrum of NO_3^- is dominant by a weak n → π* band around 302 nm ($\varepsilon = 7.2\ M^{-1}\ cm^{-1}$) and a much stronger π → π* band at 200 nm ($\varepsilon = 9900\ M^{-1}\ cm^{-1}$).[19,48] Excitation in the n → π* band ($\lambda > 280$ nm) mainly proceeds through (R2) and (R3), whereas excitation in the π → π* band ($\lambda < 280$ nm) proceeds *via* the two primary photo-processes (R2) and (R4).[19]

$$NO_3^- \xrightarrow{h\nu} [NO_3^-]^* \quad (R1)$$

$$[NO_3^-]^* \rightarrow NO_2 + O^- \xrightarrow{H_2O} NO_2 + OH + OH^- \quad (R2)$$

$$[NO_3^-]^* \rightarrow NO_2^- + O(^3P) \quad (R3)$$

$$[NO_3^-]^* \rightarrow ONOO^- \quad (R4)$$

Under atmospherically relevant irradiation (*i.e.*, >300 nm), (R2) and (R3) are more relevant, and (R4) is negligible at >280 nm. Goldstein *et al.* reported the quantum yield of $ONOO^-$ is lower than 0.2% under 300 nm illumination.[19] The pK_a (O^-/OH) is around 12, and the primary fragment O^- is immediately protonated in water to yield OH radicals.[33] OH radical is also a precursor for H_2O_2, another important oxidant in the atmosphere. However, H_2O_2 has not been detected as a significant photoproduct from nitrate photolysis at $\lambda > 200$ nm, likely due to the very low concentration and short lifetime of OH.[18]

(R3) is a potentially important source of nitrite (NO_2^-).[18] Photolysis of NO_2^- and its protonated form, nitrous acid (HNO_2), produces OH and nitric oxide (NO), which subsequently react with NO_2 or OH radicals to reproduce NO_2^-/HNO_2 (Table 1). Oxygen atoms ($O(^3P)$) react with dissolved O_2 to form O_3, which can further react with OH radicals to produce HO_2 radicals and can also react with NO_2^- to reproduce NO_3^-. Organic compounds scavenge OH radicals, and the reaction generally produces superoxide (O_2^- in Fig. 1), following subsequent reactions (Table 1). The photolysis quantum yield of (R2)

Table 1 Reactions involved in nitrate photolysis

Reactions	Rate constant	Reference
$NO_3^- + h\nu \rightarrow [NO_3^-]^*$ $(n \rightarrow \pi^*)$ $(\lambda > 280\ nm)$ $\rightarrow [NO_3^-]^*$ $(\pi \rightarrow \pi^*)$ $(\lambda < 280\ nm)$	[a]	18
$[NO_3^-]^* \rightarrow NO_2^- + O(^3P)$	[a]	18
$[NO_3^-]^* \rightarrow NO_2 + O^- \xrightarrow{H_2O} NO_2 + OH + OH^-$	[a]	18
$[NO_3^-]^* \rightarrow ONOO^- \xleftrightarrow{pK_a=6.5} HOONO$	[a]	18
$NO_2^- + h\nu \rightarrow [NO_2^-]^*$	[a]	18
$[NO_2^-]^* \rightarrow NO + O^- \xrightarrow{H_2O} NO + OH + OH^-$	[a]	18
$O^- + H_2O \leftrightarrow OH + OH^-$	$1.7 \times 10^6\ M^{-1}\ s^{-1}/1.2 \times 10^{10}\ M^{-1}\ s^{-1}$ [b]	18
$OH + NO_2 \leftrightarrow HOONO$	$1.3 \times 10^9\ M^{-1}\ s^{-1}/0.35\ s^{-1}$ [b]	18 and 19
$HOONO \rightarrow NO_3^- + H^+$	$1.4\ s^{-1}$	18
$OH + NO_2^- \rightarrow NO_2 + OH^-$	$1.0 \times 10^{10}\ M^{-1}\ s^{-1}$	18
$OH + HNO_2 \rightarrow NO_2 + H_2O$	$3.0 \times 10^9\ M^{-1}\ s^{-1}$	42
$OH + NO \rightarrow HNO_2$	$1.0 \times 10^{10}\ M^{-1}\ s^{-1}$	18
$OH + OH \rightarrow H_2O_2$	$5.5 \times 10^{10}\ M^{-1}\ s^{-1}$	21
$NO + NO_2 \rightarrow N_2O_3$	$1.1 \times 10^9\ M^{-1}\ s^{-1}$	18
$N_2O_3 + H_2O \rightarrow 2H^+ + 2NO_2^-$	$5.3 \times 10^2\ s^{-1}$	18
$NO_2 + NO_2 \rightarrow N_2O_4$	$4.5 \times 10^8\ M^{-1}\ s^{-1}$	18
$N_2O_4 + H_2O \rightarrow NO_2^- + NO_3^- + 2H^+$	$1.0 \times 10^3\ s^{-1}$	18
$NO + NO \rightarrow N_2O_2 \xrightarrow{O_2} N_2O_4$	N.A.	18
$O(^3P) + NO_3^- \rightarrow O_2NOO^- \rightarrow O_2 + NO_2^-$	$3.0 \times 10^8\ M^{-1}\ s^{-1}$	18
$O(^3P) + NO_2^- \rightarrow NO_3^-$	$3.0 \times 10^9\ M^{-1}\ s^{-1}$	18
$O(^3P) + O_2 \rightarrow O_3$	$4.0 \times 10^9\ M^{-1}\ s^{-1}$	21
$NO_2^- + O_3 \rightarrow NO_3^- + O_2$	$5.0 \times 10^5\ M^{-1}\ s^{-1}$	21
Presence of organic compounds (Org.)		
$OH + Org. \rightarrow CO_2^- \xrightarrow{O_2} CO_2 + O_2^-$	$3.8 \times 10^8\ M^{-1}\ s^{-1}$ [c]	52
$HO_2 \leftrightarrow O_2^- + H^+$	$7.9 \times 10^5\ s^{-1}/5.0 \times 10^{10}\ M^{-1}\ s^{-1}$ [b]	53
$HO_2 + O_2^- + H_2O \rightarrow H_2O_2 + O_2 + OH^-$	$9.7 \times 10^7\ M^{-1}\ s^{-1}$	54
$OH + HO_2 \rightarrow H_2O + O_2$	$9.9 \times 10^7\ M^{-1}\ s^{-1}$	53
$OH + O_2^- \rightarrow OH^- + O_2$	$1.1 \times 10^{10}\ M^{-1}\ s^{-1}$	53
$O_2^- + NO \rightarrow ONOO^-$	$4.3 \times 10^9\ M^{-1}\ s^{-1}$	55
$ONOO^- + CO_2 \rightarrow ONOOCO_2^-$	$3.0 \times 10^4\ M^{-1}\ s^{-1}$	56
$ONOOCO_2^- \rightarrow NO_3^- + CO_2$	$6.7 \times 10^5\ s^{-1}$	53
$ONOO^- + H^+ \leftrightarrow ONOOH$	$5.0 \times 10^{10}\ M^{-1}\ s^{-1}/1.2 \times 10^4\ s^{-1}$ [b]	53
$ONOOH \rightarrow NO_3^- + H^+$	$9.0 \times 10^{-1}\ s^{-1}$	53

[a] Depending on conditions such as irradiation wavelength and intensity. [b] Reverse reaction. [c] Generalized rate constant in atmospheric waters.

Open Access Article. Published on 13 de gener 2022. Downloaded on 2/2/2026 23:46:41.
This article is licensed under a Creative Commons Attribution 3.0 Unported Licence.

for OH production is 1.35 ± 0.3% at 298 K under 302 nm irradiation.[20,36,51] The quantum yield of (R3) for NO_2^- production is 1.1 ± 0.2% under 313 nm irradiation at pH > 5,[50] indicating that these two channels ((R2) and (R3)) may be of comparable importance in nitrate photolysis. These photolysis quantum yields are affected by many factors that will be discussed in Section 3.

3. Factors affecting particulate nitrate photolysis

While nitrate photolysis has been investigated for decades in laboratory experiments, theoretical studies, and field measurements, understanding how physical and environmental conditions affect particulate nitrate photolysis is far from complete. Most of the previous experimental works were performed in diluted bulk solutions, which are useful to reveal the chemistry in aqueous solutions such as in cloud droplets. However, reactions in atmospheric aerosol particles with significantly higher nitrate concentrations and surface area to volume ratios can differ from those in bulk solutions. In this section, we discuss how various factors alter particulate nitrate photochemistry.

3.1 Bulk *versus* interface: solvent cage and surface propensity

The absorption cross section of NO_3^- in aqueous solution at 310 nm is 25 times that of gas phase HNO_3 due to symmetry breaking of NO_3^- by hydration.[57] However, the water molecules surrounding NO_3^- form a solvent cage and retard nitrate photolysis. Specifically, the fragments generated from nitrate photolysis are initially surrounded by a cage of solvent (water) molecules. Their diffusion out of the cage competes with the regeneration of nitrate anions by recombining the fragments. The recombination accounts for the reduced quantum yields of nitrate photolysis in the aqueous phase compared to the gas phase.[41]

The solvent cages near the air–water interface are less complete. As a result, the recombination processes are inhibited, increasing the quantum yield of nitrate photolysis. Aerosol particles have a much larger surface area to volume ratio than bulk solutions.[8] Hence, the relative contribution of interface reactions to the overall reaction can be higher for smaller particles.[58] Furthermore, several studies have reported the surface propensities of nitrate anions at the air–water interface,[59–63] while some others reported that nitrate anions favorably reside at bulk solvation or exhibit nearly uniform distribution.[59,60,64–67] This is still a controversial topic. Therefore, more work on the surface propensity of nitrate in aerosol particles should be warranted in the future. Our experimental results showed that the surface propensity of nitrate can be enhanced by the presence of co-existing species (*i.e.*, halide ions),[37] which will be covered later.

3.2 pH

Aerosol acidity plays a critical role in atmospheric processes.[68] It affects chemical compositions, gas-particle partitioning, and toxicity[68] through various oxidation reactions, either directly or indirectly.[69,70] Here we refer acidity to as the activity of hydrogen ions or pH of aerosol particles. The inherent nitrate photolysis rate constant is not pH-dependent, and the molar light absorptivity of nitrate in aqueous solution is not sensitive to pH in the range of 2 to 6.[42] The rate of NO_2 production from nitrate thin-film photolysis is pH-independent under the atmospherically relevant pH range (pH = 0.5–6).[71] OH production from nitrate photolysis requires the protonation of O^-, but it is also insensitive at pH < 9,[20] due to its high pK_a (O^-/OH) of 12.[72]

Nonetheless, pH has significant impacts on the effective quantum yield for production of NO_2^-/HNO_2, a particular category of products with emerging oxidative potential.[11,50] Since the pK_a of HNO_2 is around 3, the speciation of NO_2^-/HNO_2 can vary; with NO_2^- dominating at pH > 3 and HNO_2 dominating at pH < 3.[73–76] Furthermore, HNO_2 or HONO is volatile with Henry's law constant of 49 ± 3 M atm^{-1} at 25 °C [77] and hence can partition from the aqueous phase into the gas phase. Scharko *et al.* found that gaseous HONO production from nitrate photolysis is the highest at the lowest pH they studied (~2) and decreases with pH, reaching almost zero at pH higher than 4, whereas gaseous NO_2 production remains constant in the pH range of 2 to 6.[42] Furthermore, Benedict *et al.* measured nitrite production and found that its quantum yield increases with pH and remains constant at pH higher than 4.5.[50] Thus, aerosol pH is the determining factor in the distribution of NO_2^-/HNO_2 in the gas phase or aqueous phase.

3.3 RH

Nitrate is hygroscopic, and the amount of water uptake is sensitive to the counter cation, particle size (Kelvin effect), and relative humidity (RH).[78] Particularly, RH is an important parameter to determine the phase of nitrate-containing particles.[79] In this section, we cover RH effects on nitrate photolysis in aqueous solutions or droplets followed by those in the solid phase.

In general, lower RH increases nitrate concentration in aqueous particles due to reduced liquid water content in the particles, leading to higher nitrate photolysis rates. However, the quantum yield of nitrate photolysis also depends on nitrate concentration. Concentrated nitrate solutions have lower quantum yields for nitrite production than diluted ones have.[80] At 310 nm irradiation and pH = 4, the quantum yield of calcium nitrate solution for nitrite production significantly decreases from $(1.4 \pm 0.1) \times 10^{-2}$ to $(4.2 \pm 0.3) \times 10^{-3}$ as nitrate concentration increases from 0.01 to 15 M. In contrast, a similar decrease was not observed in sodium nitrate solutions. This ~30 folds decrease in the nitrite quantum yield of calcium nitrate solution is attributable to the blue shift of the n–π* absorption (*i.e.*, away from actinic wavelengths) with increasing nitrate concentration. Specifically, the absorption peak of calcium nitrate solutions blue-shifts from 302 to 294 and 289 nm as the concentration increases from 0.01 to 6.0 and 14.9 M, respectively. In contrast, the blue shift for sodium nitrate solution was minimal: from 303 nm at 0.01 M to only 301 nm at 6.2 M.[80,81] In summary, higher nitrate concentration

© 2022 The Author(s). Published by the Royal Society of Chemistry

Open Access Article. Published on 13 de gener 2022. Downloaded on 2/2/2026 23:46:41.
This article is licensed under a Creative Commons Attribution 3.0 Unported Licence.

reduces the quantum yield due to the blue shift and therefore the photolysis rate constant at a given photon flux. However, it may also increase the overall nitrate photolysis rate, which is the product of nitrate concentration and nitrate photolysis rate constant.

At low RH, nitrate can exist as crystalline solids. The quantum yields of solid-phase nitrate photolysis are four orders of magnitude lower than those of aqueous phase one.[82] Nonetheless, emissions of gaseous NO_2 at >1 ppb min^{-1} [83] and HONO at < 0.06 ppt min^{-1} [84] are possible from solid-phase nitrate photolysis when thin water films or so-called surface adsorbed water (SAW) are present on the solid surface. While the exact role of SAW in nitrate photolysis remains poorly understood, the presence of SAW likely promotes the dissolution of solid nitrate to form aqueous nitrate in SAW. Because RH regulates the amount of SAW,[85] the formation of nitrate photolysis products is expected to be RH-sensitive. The increased amount of SAW might increase the availability of nitrate in its dissociated form and then enhance the quantum yields.

3.4 Temperature

Although the molar absorptivity of nitrate anion almost remains unchanged in the range of 273–298 K,[86] the quantum yields of nitrate photolysis is affected by temperature.[86–89] Specifically, the quantum yields of nitrate photolysis for production of OH, $\Phi(OH)$, and NO_2^-, $\Phi(NO_2^-)$, increase with temperature (T). Anastasio and co-workers have found the temperature dependence of the quantum yields of the two channels as $\ln(\Phi(OH)) = -(2400 \pm 480)(1/T) + (3.6 \pm 0.8)$[86] and $\ln(\Phi(NO_2^-)) = -(1330 \pm 100)(1/T) + (0.09 \pm 0.39)$.[87] According to the temperature dependence, the quantum yields for OH production can be ~0.0171 at 313 K, nearly three times that at 273 K (~0.0056). The quantum yield for nitrite production is 0.0156 at 313 K and decreases to ~0.0084 at 273 K.

3.5 Ice and snow

Nitrate photolysis on ice and snow has significant implications.[49,90,91] Nitrate can be embedded in snow pack and ice *via* deposition, heterogeneous dissolution of HNO_3(g), and freezing the water contained nitrate (*e.g.* sea and lake). Gaseous products from nitrate photolysis are observed in much higher quantities from snow packs than that from aqueous solutions.[91,92] A comprehensive review on nitrate photolysis in ice/snow is available elsewhere.[93] Here we briefly introduce the main features of nitrate photolysis on ice and snow.

Similar to the situation in the aqueous phase, nitrate photolysis on ice and snow proceeds faster at the air–snow interface than that in the bulk.[88,92] In addition to the partial solvation at the interface which allows gas phase products to easily escape, intramolecular geometrical distortion of nitrate anions at interface resulting in an increase in the absorption cross section of nitrate enhances nitrate photolysis.[92] In snow, nitrate photolysis likely occurs in the liquid like region on the surface of ice grains, or in cracks between ice grains.[94] Highly variable quantum yields of nitrate photolysis on ice and snow are reported because they are strongly influenced by the location of nitrate anions in an ice grain,[95,96] and the co-existing species (*e.g.*, Cl^-).[97] Meusinger *et al.* have proposed two photochemical domains of nitrate photolysis: photolabile nitrate anion and nitrate anion buried within the ice grain.[95] Photoproducts produced from photolabile nitrate anion can escape the ice grain and hence the quantum yields are higher than those of nitrate anion buried within the ice grain. In contrast, photoproducts from buried nitrate anions are likely to undergo a recombination reaction to regenerate nitrate anion (Fig. 1).

3.6 Effect of co-existing chemical species

Atmospheric aerosol particles consist of a myriad of different components, with diverse spatial differences, temporal variations, and distinctive source dependence.[10,98] Most laboratory studies on nitrate photolysis have used only nitrate salts without other atmospherically relevant species. The presence of co-existing chemical species has been reported to influence aqueous nitrate photolysis through (1) affecting the solvent cage effects, (2) participating in chemical reactions directly or indirectly, and (3) regulating nitrate concentration because of their hygroscopic properties determining the liquid water content. Because the last factor is reasonably well covered in the wealth of literature,[79,99] we will focus on the first two issues in this review.

3.6.1 Halides. A profound effect of inorganics on nitrate photolysis is the surface propensity of nitrate anions promoted by the coexistence of halide ions.[37,71,100,101] Halide ions are highly surface-active and hence have a surface propensity.[102–104] The presence of halide ions can lead to a preferential distribution of nitrate anions at the air–liquid interface due to the formation of a double layer of interfacial halide ions and subsurface cations that further attract nitrate anions.[43,62] The surface nitrate anions have incomplete solvent cages or the reduced solvent cage effect (Section 3.1), which gives rise to enhanced production of OH, NO, NO_2, and NO_2^-/HONO from nitrate photolysis.[43,71,100,101]

With enormous contributions from sea spray and anthropogenic sources, halide ions are ubiquitously found in atmospheric particles.[105–107] Nitrate are often internally mixed with chloride ions in the atmosphere through the chloride depletion reactions of sea spray particles. According to field measurements, the molar ratio of halides to nitrate in fresh sea spray aerosol is usually higher than 1.0,[108–112] whereas that in urban aerosol or aged marine aerosol falls in the range of 0–1.1.[113–117] Wingen *et al.* reported that the coexistence of chloride ions results in an enhanced gaseous NO_2 production from deliquesced nitrate aerosol particles under illumination by a factor of 1.6 to 2.4.[43] Zhang *et al.* found that the particulate nitrate photolysis rate constant increases by a factor of 2.0, 1.7, and 2.1 in the presence of Cl^-, Br^-, and I^-, respectively, leading to enhanced sulfate production from heterogenous oxidation of SO_2 by a factor of 1.4, 1.3, and 2.0.[37] A linear relation was found between the nitrate photolysis rate constant, $j_{NO_3^-}$, and the initial molar ratio of Cl^- to NO_3^-, $[Cl^-]_0/[NO_3^-]_0$, as $j_{NO_3^-} = 9.7 \times 10^{-5} \times [Cl^-]_0/[NO_3^-]_0 + 1.9 \times 10^{-5}$ at $[Cl^-]_0/[NO_3^-]_0$ below 0.2. No further enhancement of nitrate photolysis rate constant

Open Access Article. Published on 13 de gener 2022. Downloaded on 2/2/2026 23:46:41.
This article is licensed under a Creative Commons Attribution 3.0 Unported Licence.

was observed when $[Cl^-]_0/[NO_3^-] > 0.2$, where $j_{NO_3^-}$ can be considered the same as that at $[Cl^-]_0/[NO_3^-]_0 = 0.2$.

Compared with chloride ions, bromide and iodide ions have higher intrinsic surface propensities,[102–104] and therefore their potential impacts on the enhanced nitrate photolysis on a per molecule of halide basis are expected to be comparable or greater. However, the concentrations of bromide and iodide ions are many orders of magnitude lower than that of chloride ($[Cl^-] : [Br^-] : [I^-] = 1\,000\,000 : \sim 1515 : 1$), making them insignificant in enhancing nitrate photolysis in typical tropospheric environments.[118–120]

3.6.2 Cations. While cations do not have a pronounced effect on nitrate photolysis in the bulk phase,[50] they can influence nitrate photolysis in thin films.[83] Richards *et al.* found that thin films (~800 nm) of $RbNO_3$ and KNO_3 produce more gaseous NO_2 than those of $Mg(NO_3)_2$ and $NaNO_3$, and $Ca(NO_3)_2$.[83] Molecular dynamics simulations suggested that cations can regulate the surface propensity of nitrate anions.[66,101] For instance, the concentration of nitrate anion in the interface region of 2 M KNO_3 thin film could be ten times higher than that of 2 M $NaNO_3$. On the other hand, the formation of contact ion pairings between cation and nitrate anion[121] can reduce the quantum yields.[62] For example, $Mg(NO_3)_2$ solution produces NO_2 three times faster than $Ca(NO_3)_2$ solution because it has 50% more free nitrate at the interface, probably due to less contact ion pairings.[83] Furthermore, a recent computational study suggests that the ion pairs between cations and nitrate in an aqueous solution can also change the molar absorption coefficient, which would affect the nitrate photolysis rate.[122]

3.6.3 Organics. Organic compounds affect the formation of NO_2^-/HONO (N(III)), NO_2, and OH radicals during nitrate photolysis through three types of chemical reactions: H-donation, photosensitization, and OH scavenging. H-donation reaction directly transfers hydrogen from organic H-donors, such as organic acids and polyols, to NO_2 to form N(III).[123] On the other hand, photosensitization triggered by light-absorbing organic species, such as aromatic carbonyls and humic-like substances, can indirectly convert NO_2 to HONO. The light-absorbing organics or photosensitizers absorb light and transfer from their ground state to the singlet excited state. Some molecules (*e.g.*, aromatic carbonyl) at the singlet excited state will be converted to the triplet excited state. The triplet excited state of organic species has a longer lifetime, allowing for interactions/reactions with H donors to form ketyl radicals, which can react with NO_2 to yield HONO.[124–127] The H-donation reaction and the photosensitization can enhance production rates of photoproducts during nitrate photolysis. For example, Yang *et al.* reported that the gaseous HONO emission from irradiated thin films containing nitrate and humic acid reached 16 ppt h^{-1}, whereas the upper limit without humic acids was just 3.6 ppt h^{-1}.[84] Ye *et al.* premixed HNO_3 solutions with organic acids, polyols, and aromatic compounds and found that the co-existing organics can enhance the photolysis rate constant of HNO_3 adsorbed on Pyrex glass surface by up to one order of magnitude *via* H-donation reactions and photosensitization.[123] Furthermore, our latest work reported the enhanced nitration (Section 5.3) of vanillin by increased NO_2 formation from nitrate photolysis. The increased NO_2 formation results from the reaction of nitrite with superoxide and OH radicals produced from photosensitizing reactions of vanillin.[135]

Organic compounds are highly reactive toward OH radicals and increase the effective quantum yields for NO_2 production by suppressing the NO_2 consuming reaction between NO_2 and OH radicals.[50] Scavenging of OH radicals can also increase the quantum yields for N(III) production in two ways. Firstly, organic scavengers reduce N(III) oxidation loss by OH radicals by consuming them. Second, some organics such as ethylene glycol and glyoxal react with OH radicals to form O_2^-/HO_2 radicals, which can further lead to secondary formation of N(III) from the $NO_2 + O_2^-/HO_2$ reaction.[11,42,128]

It is found that HONO emissions from nitrate photolysis are enhanced by dissolved aliphatic organic matter through enhanced production of superoxide.[128] Wang *et al.* demonstrated the importance of solvated electrons produced from photosensitizing reactions in enhanced nitrite production from nitrate photolysis.[158] They suggested that the solvated electrons are mainly scavenged by nitrate, leading to more NO_2 production for further conversion to nitrite.

Highly viscous organic materials could hinder reactions in the particle phase. Liang *et al.* examined nitrate photolysis in mixed sucrose–nitrate–sulfate particles as a proxy of viscous aerosol particles.[129] They found the suppressed nitrate crystallization by the presence of sucrose and the high photolysis rate constants ($\sim 10^{-5}$ s^{-1}), irrespective of the RH. They observed the formation of enlarged hollow semisolid particles at high sucrose content and low RH, likely due to the release of gaseous species like NO_2/HONO pushing the viscous materials radially outward. Thus, particulate nitrate photolysis may affect the microphysics of aerosol particles.

3.7 Mie resonances of droplets

Light intensity is a crucial parameter in determining nitrate photolysis rates. In the photochemistry of micrometer-sized spherical droplets, the actinic flux in the droplet can be enhanced due to (i) the Mie resonances, also known as the whispering gallery mode resonances, or the morphology-dependent resonances (MDRs), and (ii) the increased light pathlengths in the droplets.[41,130,131] MDRs, characterized in terms of the size parameter (*i.e.*, particle diameter × π/wavelength), have been studied in the physical and chemical characterization of aerosols, especially in laboratory studies including elastic scattering, fluorescence, and Raman spectroscopy.[132] Although MDRs can yield the orders of magnitudes increase in the internal actinic flux, their contribution to the actinic flux enhancement is not profound when averaged over typical droplet size distributions.[130,133] Under broadband solar irradiation (290–600 nm), MDRs and the increased light pathlengths in ~2 μm droplet can produce a ~2-fold intensity enhancement (2.06 in 1-decene; 1.76 in pure water) in spherical aqueous droplets relative to bulk-liquid solutions.[130,131] However, the role of Mie resonances in enhancing nitrate photolysis has not been experimentally ascertained.

© 2022 The Author(s). Published by the Royal Society of Chemistry

Open Access Article. Published on 13 de gener 2022. Downloaded on 2/2/2026 23:46:41.
This article is licensed under a Creative Commons Attribution 3.0 Unported Licence.

3.8 Mineral dusts

Mineral dusts are one of the most significant contributors to aerosol mass, with an estimated annual emission of 1000–3000 Tg.[134] Recent work reported a synergistic effect of iron–organic complexes and nitrate photolysis in nitrite/nitrous acid generation.[159] Previous studies explored nitrate photolysis on the surface of mineral oxides: (1) non-photoactive oxides (NPO; *e.g.*, Al_2O_3, SiO_2) and (2) photoactive semiconductive oxides (PSO; *e.g.*, TiO_2). Generally speaking, both NPO and PSO provide numerous surface reactive sites for the adsorption of nitrate.[136–138] Spectroscopic analysis revealed that the interactions between HNO_3/nitrate and reactive surface sites could distort the molecular structure of HNO_3/nitrate, which results in a red shift in n → π* absorption and an increase of light absorption cross section relative to gas-phase HNO_3.[136,139,140] Additionally, PSO have excellent photocatalytic capacity *via* an electron–hole conductive mechanism.[8,14] In ambient environment, the adsorbed oxygen (O_2) accepts an electron to produce highly reactive O_2^-, facilitating nitrate adsorption and subsequent photoreactions.[8]

While nitrate photochemistry on oxide surfaces has been widely investigated, aluminosilicates, which can account for >70% of dust mass, are rarely explored.[141] Using NaY zeolite as a model system of aluminosilicates, Gankanda and Grassian found that its photoactivity may be significantly different from the non-photoactive and photoactive oxides.[142,143] N(III) produced from nitrate photolysis can stably exist as the primary product inside the zeolite cage during nitrate photolysis, whereas nitrate photolysis on oxide surfaces mainly produces gaseous NO_2. Hence, porous materials in mineral dust can potentially act as a platform for producing daytime gaseous HONO.

4. Quantum yields and photolysis rate constants

The impacts of particulate nitrate photolysis in atmospheric chemistry rely highly on its quantum yields or photolysis rate constants. They are the parameters required for implementing particulate nitrate photolysis mechanisms in air quality modeling.[13] They are relatively well constrained for the gas phase and aqueous (bulk) phase photolysis,[6,144] but not for particulate nitrate. This section summarizes the reported quantum yields and photolysis rate constants of nitrate (Tables 2 and 3, respectively) to discuss the current understanding of nitrate photolysis rate constants.

4.1 Nitrate photolysis rate constants of ambient aerosol particles

Most works reported that nitrate photolysis rate constants of ambient particles ranged from 10^{-5} to 10^{-4} s^{-1},[38,145,146] which are 100–1000 times that of aqueous solution and gaseous HNO_3.[18] Ye *et al.* measured nitrate photolysis rate constants of ambient particles collected at different locations in North

Table 2 Quantum yields, Φ, of nitrate photolysis

Sample	Nitrate concentration	Φ (%) for NO_2^- production	pH	OH scavenger	Irradiation wavelength	Note/reference
$NaNO_3$ aqueous solution	50 μM	0.93 ± 0.1	5.2	500 μM 2-propanol	313 nm	88
$NaNO_3$ aqueous solution	50 μM	1.1 ± 0.2	≥5	None	313 nm	50
		<0.26[a]		50 μM formate		
		1.18 ± 0.14		50 μM cysteine		
		1.16 ± 0.04				
$Ca(NO_3)_2$	50 μM	1.01–1.20	7.3–7.52	None	313 nm	50
$Mg(NO_3)_2$		0.99–1.06	7.2–7.58			
NH_4NO_3		0.9 ± 0.1	7.14–7.39			
KNO_3		1.16 ± 0.13	7.35–7.4			
$NaNO_3$ aqueous solutions	0.01 M	0.45	4	None	310 nm	80
	0.1 M	0.35				
	1.4 M	0.62				
	5.1 M	0.25				
$NaNO_3$ aqueous solutions	0.01 M	0.80	4	10 mM formate	310 nm	80
	0.1 M	1.13				
	1.4 M	0.92				
	5.1 M	1.25				
KNO_3 aqueous solution	0.1 M	0.65 ± 0.04	N.A.	0.5 M formate	310 nm	160
		0.60 ± 0.04		0.34 M EtOH	313 nm	
$NaNO_3$ aqueous solution	0.02–1 M	0.94 ± 0.02	4.2–4.5	10 mM formate	300 nm	19
$NaNO_3$ aqueous solution	0.01 M	0.72 ± 0.09[b]	3.0	0.13 M 2-propanol	305 nm	51
		1.00 ± 0.04	4.0			
		1.02 ± 0.07	5.6			
		1.24 ± 0.14	9.0			
		1.22 ± 0.07	11.0			
KNO_3 aqueous solution	3 mM	1.7 ± 0.3[b]	4–9	0.3 M thiocyanate	308 nm	20

[a] Quantum yields for $ONOO^-$ production. [b] Quantum yields for OH production.

Open Access Article. Published on 13 de gener 2022. Downloaded on 2/2/2026 23:46:41.
This article is licensed under a Creative Commons Attribution 3.0 Unported Licence.

Table 3 Reported nitrate photolysis rate constants, j_{NO3^-}, for various nitrate samples

Sample type (particle size)[a]	$j_{NO_3^-}$ (s^{-1})	Species used for estimating $j_{NO_3^-}$	Irradiation wavelengths	Note/reference
Ambient aerosol	$(6.1 \pm 4.2) \times 10^{-5}$	Gaseous NO_2 and HONO	>290 nm	Albany, NY(urban)/[38]
Ambient aerosol	$(1.5 \pm 1.2) \times 10^{-4}$	Gaseous NO_2 and HONO	>290 nm	Delmar, NY (suburban)/[38]
Ambient aerosol	$(2.3 \pm 2.4) \times 10^{-4}$	Gaseous NO_2 and HONO	>290 nm	Whiteface mountain summit, NY (remote areas)/[38]
Ambient aerosol	$(1.9 \pm 1.2) \times 10^{-4}$	Gaseous NO_2 and HONO	>290 nm	Aircraft measurements in southeast US/[38]
HNO_3/nitrate on building material surfaces	$(6.0 \pm 5.3) \times 10^{-5}$	Gaseous NO_2 and HONO	Natural sun light or Hg lamp	147
HNO_3/nitrate on plant leaf surfaces	$(6.0 \pm 8.7) \times 10^{-5}$	Gaseous NO_2 and HONO	Natural sun light or Hg lamp	147
HNO_3/nitrate on urban grime	$(2.7 \pm 1.0) \times 10^{-4}$ to $(5.4 \pm 2.7) \times 10^{-4}$	Nitrate	>290 nm	148
Nitrate aerosol (80 nm)	3×10^{-6} for UVA; 2×10^{-5} for UVB	Gaseous NO_2, NO, and HONO	UVA and UVB	Laboratory generated/[39]
Ambient aerosol	1.0×10^{-4}	Gaseous NO_2, and HONO	>300 nm Xenon lamp	Clean marine boundary layer/[40]
AN (25 μm)	1.0×10^{-7}	Sulfate as oxidation product	250 nm mercury lamp	Laboratory generated droplets/[12]
AN (~50 μm)	7.4×10^{-6}	Sulfate as oxidation product	300 nm LED	Laboratory generated droplets/[11]
AN/Gly	2.7×10^{-5}			
AN/OA	3.0×10^{-5}			
AN/SBC	2.7×10^{-6}			
AN (~50 μm)	2.0×10^{-5}	Sulfate as oxidation product	300 nm LED UV lamp	Laboratory generated droplets/[37]
AN/chloride	4.0×10^{-5}			
AN/bromide	3.4×10^{-5}			
AN/iodide	7.5×10^{-5}			
Nitrate solution	$(1.23 \pm 0.04) \times 10^{-7}$	Reaction products of benzoic acid and OH radicals	>290 nm Xenon lamp	161
Nitrate solution	$\sim 3.0 \times 10^{-7}$	Reaction products of benzoic acid and OH radicals	Natural sunlight	144

[a] AN: ammonium nitrate; Gly: glyoxal; OA: oxalic acid; SBC: sodium bicarbonate.

America. They reported the mean values of 6.1 ($\pm$4.2) $\times$ 10^{-5} s^{-1} for samples collected in Albany, NY (urban area), 1.5 ($\pm$1.2) $\times$ 10^{-4} s^{-1} in Delmar, NY (rural area), 2.3 ($\pm$2.4) $\times$ 10^{-4} s^{-1} from Whiteface Mountain summit (remote area), and 1.9 ($\pm$1.2) $\times$ 10^{-4} s^{-1} from flight sampling.[38] Bao *et al.* reported the nitrate photolysis rate constants of ambient particles sampled in Beijing from 1.2 $\times$ 10^{-5} to 4.8 $\times$ 10^{-4} s^{-1}.[145] In contrast, Romer suggested the particulate nitrate photolysis rate constants of 7 $\times$ 10^{-6} to 2.1 $\times$ 10^{-5} s^{-1}, 10–30 times higher than that of gas-phase HNO_3, based on the aircraft observations over South Korea.[146] On the other hand, Shi *et al.* found a limited role in the photolysis of particulate nitrate for gaseous NO_x and HONO production.[39] Nitrate photolysis rate constants on building material surfaces, plant leaf surfaces, and urban grime have been reported to be 6.0 ($\pm$5.3) $\times$ 10^{-5} s^{-1}, 6.0 ($\pm$8.7) $\times$ 10^{-5} s^{-1} and 1.2 $\times$ 10^{-3} s^{-1}, respectively.[144,147,148] Furthermore, Laufs and Kleffmann reported a very low HNO_3 photolysis rate constant on quartz surfaces for HONO formation, implying the negligible contribution of nitrate photolysis to the daytime HONO sources.[149] The contradictory results related to HNO_3 surface photolysis were also reported, highlighting the importance of HNO_3 coverage on solid surfaces in the absence *versus* in the presence of water vapor.[150] Thus, the rate constants in the atmosphere are highly variable and uncertain.

4.2 Estimation of particulate nitrate photolysis rate constant

There is a growing body of research on the enhancement of particulate nitrate photolysis. Accurate estimation of nitrate photolysis rate constant is key to quantifying atmospheric relevance of enhanced particulate nitrate photolysis. The particulate nitrate photolysis rate constant, $j_{pNO_3^-}$, is a first order decay rate constant:

$$-\frac{d[NO_3^-]}{dt} = j_{pNO_3^-}[NO_3^-] \quad (1)$$

One way to measure $j_{pNO_3^-}$ is to quantify the decay of nitrate.[148] However, it is challenging due to its small value of reported $j_{pNO_3^-}$: $10^{-6} \sim 10^{-4}$ s^{-1}. For instance, it takes about 12 days to see the nitrate decrease by 1 M at $j_{pNO_3^-}$ of 10^{-6} s^{-1}. Hence, studies on the direct measurements of nitrate decay are scarce (Table 3). In addition, this estimation may be complicated by regeneration reactions of nitrate during nitrate photolysis (Table 1), but the effect of the regeneration reaction (OH + NO_2) on the quantification of $j_{pNO_3^-}$ would be minimized in the presence of OH scavengers. Another estimation method measures the gas phase photoproducts of nitrate photolysis such as NO_2, and HONO,[39] assuming low concentrations in the particle phase given their low Henry's law constants:[151]

© 2022 The Author(s). Published by the Royal Society of Chemistry

Open Access Article. Published on 13 de gener 2022. Downloaded on 2/2/2026 23:46:41.
This article is licensed under a Creative Commons Attribution 3.0 Unported Licence.

$$j_{\mathrm{pNO_3^-}} = \sum_i P_{i,\mathrm{gas}} / N_{\mathrm{nitrate}}, \quad (2)$$

where $P_{i,\mathrm{gas}}$ and N_{nitrate} are the production rate of a given gaseous photoproduct generated from nitrate photolysis and the amount of particulate nitrate exposed to light, respectively. As shown in Table 3, the measurements of gaseous photoproducts have been used to estimate $j_{\mathrm{pNO_3^-}}$ in most studies. Gaseous NO_2 and HONO are the main target photoproducts. However, estimations based on the gaseous photoproduct measurements may underestimate $j_{\mathrm{pNO_3^-}}$ because they do not include production rates of in-particle NO_2 and NO_2^-/HNO_2. Gaseous photoproducts are generated only when in-particle photoproducts partition into the gas-phase. The in-particle photoproducts are subjected to secondary reactions in the particle phase due to the presence of many reactive species, as will be described in Section 5. If the secondary reactions in the particle phase are fast, the photoproducts can be almost entirely consumed before leaving the particle phase into the gas phase, leading to no or low production of gaseous photoproducts and underestimation of $j_{\mathrm{pNO_3^-}}$. To the best of our knowledge, there are no simultaneous measurements of gas and particle-phase photoproducts to better constrain $j_{\mathrm{pNO_3^-}}$.

UV irradiance fluctuates daily and seasonally as a function of latitude, solar zenith angle, cloud cover, and stratospheric ozone and particle concentrations.[144] $j_{\mathrm{pNO_3^-}}$ is related to the wavelength-dependent photon fluxes received by particulate nitrate, $I_{\mathrm{pNO_3^-}}(\lambda)$, the molar absorptivity, $\varepsilon_{\mathrm{NO_3^-}}(\lambda)$, and the quantum yield, $\phi_{\mathrm{NO_3^-}}(\lambda)$:

$$j_{\mathrm{pNO_3^-}} = \frac{\ln(10) \times 10^3}{N_A} \int \varepsilon_{\mathrm{NO_3^-}}(\lambda) \times \phi_{\mathrm{NO_3^-}}(\lambda) \times I_{\mathrm{pNO_3^-}}(\lambda) \mathrm{d}\lambda, \quad (3)$$

where N_A is the Avogadro's number. Values of $\varepsilon_{\mathrm{NO_3^-}}(\lambda)$ are well known.[86] In contrast, the photon fluxes and quantum yields for particulate nitrate can be significantly different from those for bulk nitrate solutions, as discussed in Section 3. Table 2 lists the reported quantum yields, and they are less variable (0.25–1.7) than $j_{\mathrm{pNO_3^-}}$, because only studies of quantum yield from bulk solutions are available. The values of $j_{\mathrm{pNO_3^-}}$ are highly variable (Table 3), partly because of various light sources with different wavelengths and intensities used in earlier work in addition to the complicated processes of particulate nitrate photolysis (Section 3). For better comparison of the experimentally determined $j_{\mathrm{pNO_3^-}}$ among studies, it can be normalized to that under the typical tropical summer conditions on the ground using the following equation:[40]

$$j^{\mathrm{N}}_{\mathrm{pNO_3^-}} = j_{\mathrm{pNO_3^-}} \times \frac{j_{\mathrm{nitrate,0}}}{j_{\mathrm{nitrate}}} \quad (4)$$

where $j^{\mathrm{N}}_{\mathrm{pNO_3^-}}$ is the $j_{\mathrm{pNO_3^-}}$ normalized to the typical tropical summer condition; $j_{\mathrm{nitrate,0}}$, and j_{nitrate} are the photolysis rate constants of an aqueous solution under the typical tropical summer conditions and that exposed to the experimental photon fluxes, respectively. A value of 3.0×10^{-7} s^{-1} can be used for $j_{\mathrm{nitrate,0}}$.[6] Reporting $j^{\mathrm{N}}_{\mathrm{pNO_3^-}}$ based on $j_{\mathrm{pNO_3^-}}$ is recommended for a quantitative comparison of experimental results obtained under different conditions.

Besides nitrate, many other light-absorbing species such as black carbon[152] and brown carbon[153] exist, and they can be internally mixed with nitrate in atmospheric particles.[154,155] The incident photon flux, $I(\lambda)$, is then absorbed by nitrate as well as those light-absorbing species in the particle phase. The spectral photon fluxes absorbed by a component (i), $I_{\mathrm{ai}}(\lambda)$, in light-absorbing multicomponent mixtures is written by

$$I_{ai}(\lambda) = \frac{\varepsilon_i(\lambda) c_i l}{\sum_i \varepsilon_i(\lambda) c_i l} [1 - T(\lambda)] I(\lambda), \quad (5)$$

where $\varepsilon_i(\lambda)$ and c_i are the wavelength-dependent molar absorptivity and the concentration of species i, respectively; l and $T(\lambda)$ are the light path length and the wavelength-dependent transmission of a species i, respectively. Eqn (5) illustrates that the fraction of photon fluxes absorbed by nitrate in the particle phase, $I_{\mathrm{pNO_3^-}}(\lambda)$, decreases with increasing concentrations of other light-absorbing species. Hence, quantifying the total adsorbed photon fluxes, $\sum_i \varepsilon_i(\lambda) c_i l$, is crucial to constrain $j_{\mathrm{pNO_3^-}}$. Given that the sources and chemical compositions of brown carbon remain to be understood,[153,156,157] the total adsorbed photon fluxes, $\sum_i \varepsilon_i(\lambda) c_i l$, are highly uncertain. Studies of brown carbon in association with particulate nitrate photolysis are warranted.[135,179] Note that eqn (5) assumes homogeneous mixing. If a nitrate particle was covered by light-absorbing species (*e.g.*, through liquid–liquid phase separation[129]), such a screening effect would be intensified.

5. Nitrate-photolysis-initiated reactions

As discussed in Section 2, particulate nitrate photolysis produces strong in-particle oxidants of OH, NO_2, NO_2^-/HNO_2, and O_3, and they will initiate a series of reactions in the particle phase.[162–164] Note that reactions induced by OH radicals are not only specific to nitrate photolysis, but also the other OH sources such as phase transfer from gas phase and H_2O_2 photolysis.[165] This section reviews studies of the following reactions promoted by particulate nitrate photolysis: multiphase oxidation of (1) SO_2 and (2) organic compounds, and (3) the formation of nitrated products in the aqueous phase of deliquesced aerosols and cloud droplets.

5.1 Multiphase oxidation of SO_2

Particulate nitrate photolysis has recently been found to promote multiphase SO_2 oxidation by generating OH, NO_2, and NO_2^-/HONO (Fig. 2).[11,12,37] SO_2 is dissolved in aerosol liquid water and is present as bisulfite or/and sulfite depending on the pH of the particle. Under typical acidic conditions (pH < 6), dissolved SO_2 mainly exists as bisulfite.[2] Bisulfite can react with all OH, NO_2, and NO_2^-/HONO for sulfate production. O_3 is also possible to oxidize bisulfite,[2] but this oxidation mechanism was not efficient in our previous study.[11] The reaction of bisulfite and OH radical forms the sulfite radical anion, which initiates

Open Access Article. Published on 13 de gener 2022. Downloaded on 2/2/2026 23:46:41.
This article is licensed under a Creative Commons Attribution 3.0 Unported Licence.

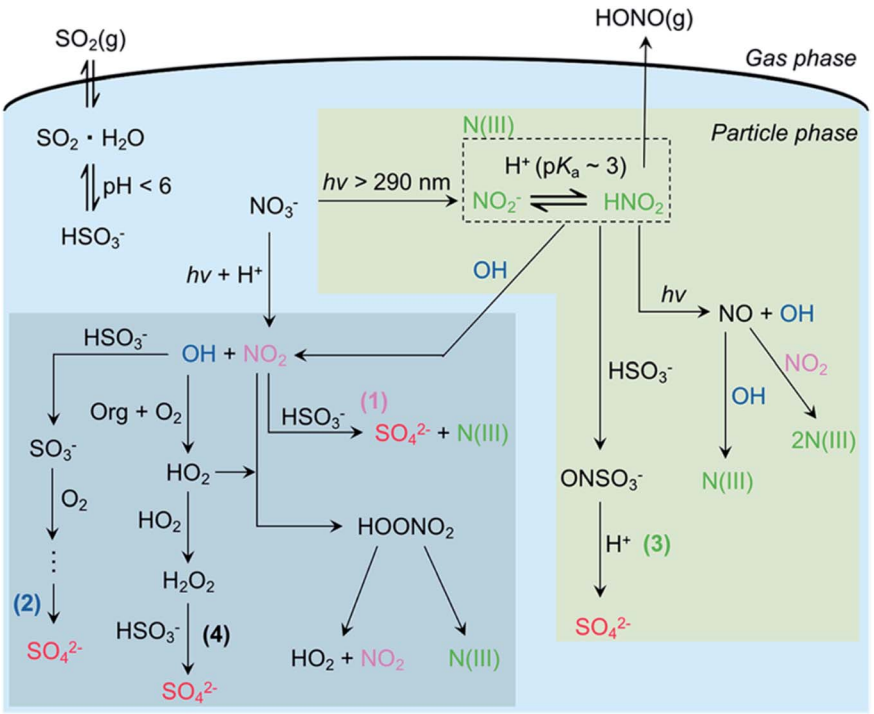

Fig. 2 Proposed multiphase oxidation of SO_2 promoted by particulate nitrate photolysis. Reprinted with permission from ref. 11 Copyright 2019 American Chemical Society.

the chain reactions involving SO_5^-, HSO_5^-, and SO_4^- in the presence of dissolved O_2 to produce multiple sulfate ions from each attack of OH on dissolved SO_2.[2] The oxidation by dissolved NO_2, one of the most feasible mechanisms during the haze events,[166] is a one-step process. During particulate nitrate photolysis at 300 nm, the highest sulfate production is found from the oxidation by NO_2^-/HONO, compared to the other oxidation mechanisms such as OH and NO_2 radicals. A simple parameterization of sulfate production results using the reactive uptake coefficient of SO_2, γ_{SO_2}, and nitrate photolysis rate, $P_{NO_3^-}$, gives the following relation: $\gamma_{SO_2} = 1.64 \times P_{NO_3^-}$.[11] Given that nitrate concentration is as high as 10 M under highly polluted episodes and much faster particulate nitrate photolysis than that in aqueous solution,[8,38,167] γ_{SO_2} can become $>10^{-5}$, which is comparable to the values necessary for explaining the observations in the haze events in China.[168]

5.2 Multiphase oxidation of organics in aqueous phase secondary organic aerosol formation

Organic aerosol accounts for about 20–90% of the total particulate matter on a global scale.[10] A significant fraction of this organic matter is secondary, *i.e.*, formed in the atmosphere by converting gases into the condensed matter.[169] The in-particle OH radicals produced from nitrate photolysis can promote the formation of aqueous-phase secondary organic aerosol (SOA). In aqueous aerosol particles or cloud droplets, OH radicals oxidize dissolved organic compounds such as glyoxal and methylglyoxal, pyruvic acid, glycolaldehyde, methacrolein, methyl vinyl ketone, and acetone, yielding both low-molecular-weight products (*e.g.*, dicarboxylic acids) and high-molecular-weight compounds (*e.g.*, oligomers).[170–174] Aqueous SOA yields from the photo-oxidation of phenolic carbonyls in nitrate solution are twice as high as those in sulfate solution due to the efficient generation of OH through nitrate photolysis.[175] Our recent work examined the role of particulate nitrate photolysis in the formation of SOA from particle-phase oxidation of glyoxal by OH radicals.[176] Interestingly, we did not observe typical oxidation products such as oxalic acid, glyoxylic acid, and higher-molecular-weight products previously reported in the literature. Instead, formic acid/formate was the main oxidation product. In the presence of ammonium as a source of dissolved ammonia, light-absorbing species are formed[177,178] and trigger the photosensitization reactions to promote glyoxal oxidation.[179] Particulate nitrate photolysis can alter major reaction pathways of glyoxal oxidation.

5.3 Nitration for browning atmospheric aerosol

Nitration is a chemical process that introduces a nitro group into an organic compound. The nitration of aromatic compounds has gained attention as an emerging process to produce light-absorbing organic matter or brown carbon (BrC) in the atmosphere.[153,180–190] It can also chemically modify allergenic proteins present in the atmosphere (*e.g.*, amino-acid tyrosine) and enhance their allergenicity.[191–195] Nitrate photolysis is a potential contributor to the nitration process for browning atmospheric aerosol[175,181,182,189] and increasing the allergenicity[196] by producing nitrating agents of NO_2/N_2O_4, nitrite (NO_2^-), nitrous acid (HNO_2), and peroxynitrous acid (HOONO).[197]

© 2022 The Author(s). Published by the Royal Society of Chemistry

Open Access Article. Published on 13 de gener 2022. Downloaded on 2/2/2026 23:46:41.
This article is licensed under a Creative Commons Attribution 3.0 Unported Licence.

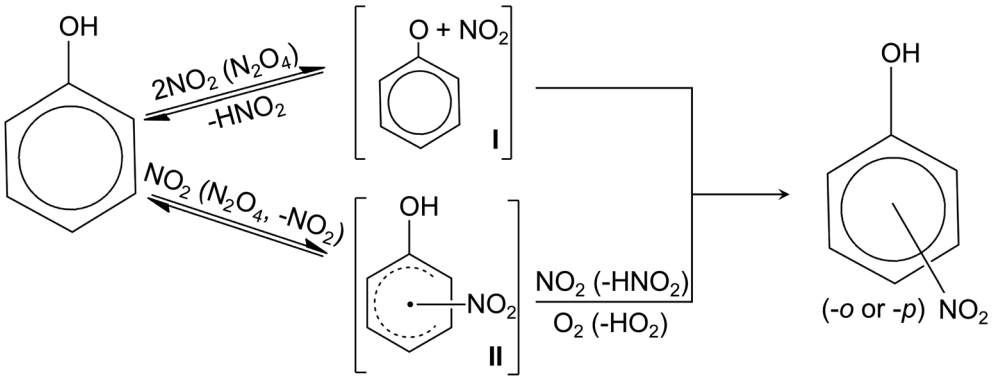

Fig. 3 Proposed reaction mechanisms for phenol nitration.[213,214]

Nitration by NO_2 has been reported for aromatic compounds such as phenols,[198–200] methoxyphenols,[181,182,189] benzene,[201] toluene,[202] and catechols.[203] Phenols are important precursors for SOA formation, including BrC.[204,205] Among the major nitrated aromatic compounds (NACs) found in the atmosphere are nitrophenols, nitrocatechols, nitrosalicylic acids, and nitroguaiacols.[180,184,185] NACs and their derivatives contribute to 50–80% of the total visible light absorption by BrC emitted from biomass burning,[206] with mass absorption coefficients (MAC) ranging from 0.05 to 4 $m^2\ g^{-1}$.[206–208] NACs can be directly emitted into the atmosphere such as by traffic exhaust,[209] and biomass burning,[210] and secondarily formed by the nitration of aromatic precursors in both the aqueous and the gas phases.[189,201,211]

Nitrophenol is one of the most abundant nitrated organic species in the atmosphere.[206] The most prominent atmospheric process for nitrophenol formation is the nitration of phenol.[212] Fig. 3 summarizes the proposed reaction mechanisms for the nitration of phenol.[213,214] Nitration is initiated by the reaction between phenol and two NO_2 (or N_2O_4) (Fig. 3) *via* H-atom abstraction or electrophilic addition to the ring, resulting in a radical intermediate which is either a phenoxyl (**I** in Fig. 3)[215] or hydroxynitrocyclohexadienyl (**II**).[216] The phenoxyl (**I**) can react with either OH radicals to form hydroxyderivatives (*e.g.*, catechol and hydroquinone, resorcinol to a lesser extent) or with NO_2 to yield nitrophenols.[213] Contrastingly, hydroxynitrocyclohexadienyl (**II**) can undergo H-atom abstraction by O_2 or another NO_2 to form nitrophenols.[200,216] While other pathways of nitrophenol formation are possible,[199,200,215,217] the nitration of phenol *via* nitrate photolysis in the atmosphere (the presence of oxygen) primarily proceeds through the hydroxynitrocyclohexadienyl (**II** in Fig. 3).

Nitration of phenols by NO_2 is enhanced in the presence of OH scavengers such as 2-propanol.[213] Scavengers inhibit the recombination of OH with NO_2 to regenerate NO_3^- + H^+,[218] allowing more NO_2 available for the nitration of phenol. The formation of nitrated phenols *via* nitrate photolysis was observed to decrease with increasing pH.[213] At high pH, N_2O_4 can react with OH^- to form NO_3^- and NO_2^-. At pH < 3, the formation of nitrophenols can be enhanced by thermal reactions (*i.e.*, in the dark) involving HNO_2.[219,220] An example is the HNO_2-catalyzed phenol nitration in which phenol directly reacts with N(III) (HNO_2 or N_2O_3) in the dark.[220] Although the reaction between phenol and HNO_2 or N_2O_3 is a thermal process, nitrate irradiation is required to generate nitrite.

HOONO, an isomer of nitric acid (HNO_3), is formed upon nitrate photoisomerization (R4). It is a powerful nitrating agent for both phenolic and non-phenolic aromatic substrates such as phenol, benzene, and naphthalene.[201,221,222] Although the direct formation of HOONO upon nitrate irradiation requires wavelength that is not atmospherically relevant (<290 nm), it can also be generated from HNO_2 and NO produced from nitrate photolysis *via* the reaction between NO and O_2^-.[221] The irradiation of solid nitrate salts (NH_4NO_3, $NaNO_3$) with benzene can also yield phenol and nitrobenzene, possibly due to the generation of OH and NO_2.[212,223] In the presence of hematite (α-Fe_2O_3),[224] significant enhancement in nitrobenzene formation occurs likely due to the protonation of peroxynitrite (formed upon nitrate photoisomerization) to HOONO.[225]

6. Future directions

We have discussed the potential impacts of particulate nitrate photolysis in the atmosphere. Yet, many issues remain unresolved. Here, we propose the following questions to be addressed to better constrain the impacts of particulate nitrate photolysis.

(1) How much can particulate nitrate photolysis promote multiphase oxidation for the secondary formation of inorganic and organic compounds in the particles, respectively? Earlier works have mainly studied the production of gaseous photoproducts of NO_2 and HONO from nitrate photolysis (Table 3). Particular attention needs to be paid to quantifying the oxidation capacity of particulate nitrate photolysis in the particle phase. While gas phase chemistry is not the focus of this paper, particulate nitrate photolysis can affect gas phase chemistry by producing NO_x. The NO_x recycling from particulate nitrate photolysis can lead to enhancements in NO_x, OH, and O_3 concentrations in the atmosphere.[34] It is also possible that photolysis of organic nitrates could influence the nitrogen cycle and O_3 production, but there are very few studies on this topic.[47]

(2) What roles does particulate nitrate photolysis play in the formation and aging of brown carbon aerosols? Nitrate has

Open Access Article. Published on 13 de gener 2022. Downloaded on 2/2/2026 23:46:41.
This article is licensed under a Creative Commons Attribution 3.0 Unported Licence.

been recognized as a nitrating agent in brown carbon formation.[226] On the other hand, nitrate photolysis has the potential to accelerate the aging of brown carbon.[175] Nonetheless, studies on both the formation and aging of brown carbon during particulate nitrate photolysis are scarce.

(3) What is the role of the surface/interfacial effects (Sections 3.1 and 3.6.1) in promoting nitrate photolysis in the particle phase? When nitrate anions are localized at the air/particle interface, they are not fully solvated. Nitrate photolysis in the incomplete solvent cage can proceed faster than in the complete solvent cage, which is one of the plausible reasons to differentiate nitrate photolysis in the particle phase from bulk solutions. However, whether nitrate anions are so surface-active to affect the rate constant in particles is still controversial. What makes nitrate photolysis in particles so different from in bulk solutions needs to be elucidated.

(4) What parameters best describe particulate nitrate photolysis in air quality models? The photolysis rate constants are one of the most practical parameters that can be used in air quality models to implement particulate nitrate photolysis. The majority of studies have measured photoproducts of gaseous species such as NO_2 and HONO to estimate the rate constants. However, this method might potentially underestimate the constants (Section 4). Measurements of both gas and particle phase photoproducts generated from particulate nitrate photolysis are recommended to better constrain the rate constants. In addition to the photolysis rate constants, the branching ratio of photoproducts N(III) to NO_2 is also an important parameter that affects the product yields during nitrate photolysis. A N(III) : NO_2 molar ratio of 0.33–0.67 was assumed in earlier modeling works.[40,227] However, the product yields can be affected by many factors as discussed in Section 3. Systematic studies under more realistic complex aerosol systems such as nitrate particles internally mixed with black carbon, BrC, radical scavengers, surface-active species (*e.g.*, halide ions), and heterogeneously mixed (*e.g.*, liquid–liquid phase separated) particles are needed.

Author contributions

Masao Gen: conceptualization, organization, data analysis, writing–original draft, writing–review & editing. Zhancong Liang: writing–original draft, writing–review & editing. Ruifeng Zhang: writing–original draft, writing–review & editing. Brix Raphael Go: writing–original draft, writing–review & editing. Chak K. Chan: conceptualization, organization, data analysis, writing–original draft, writing–review & editing

Conflicts of interest

There are no conflicts of interest to declare.

Acknowledgements

We gratefully acknowledge support from the National Natural Science Foundation of China (42075100 and 41875142), the Guangdong Basic and Applied Basic Research Foundation (2020B1515130003), the Japan Science and Technology Agency (JST) for Fusion Oriented Research for disruptive Science and Technology program (JPMJFR206V), the Japan Society for the Promotion of Science (JSPS) Grants-in-Aid for Early-Career Scientists (21K17876).

References

1 X. Y. Boucher, O. Randall, D. Artaxo, P. Bretherton, C. Feingold, G. Forster, P. Kerminen, V. M. Kondo, Y. Liao, H. Lohmann, U. Rasch, P. Satheesh, S. K. Sherwood, S. Stevens and B. Zhang, *Climate Change 2013: the Physical Science Basis. Contribution of Working Group I to the Fifth Assessment Report of the Intergovernmental Panel on Climate Change*, Cambridge University Press, New York, 2013.

2 J. H. Seinfeld and S. N. Pandis, *Atmospheric Chemistry and Physics: from Air Pollution to Climate Change*, Wiley, New York, 2006.

3 M. Hallquist, J. C. Wenger, U. Baltensperger, Y. Rudich, D. Simpson, M. Claeys, J. Dommen, N. M. Donahue, C. George, A. H. Goldstein, J. F. Hamilton, H. Herrmann, T. Hoffmann, Y. Iinuma, M. Jang, M. E. Jenkin, J. L. Jimenez, A. Kiendler-Scharr, W. Maenhaut, G. McFiggans, T. F. Mentel, A. Monod, A. S. H. Prévôt, J. H. Seinfeld, J. D. Surratt, R. Szmigielski and J. Wildt, *Atmos. Chem. Phys.*, 2009, **9**, 5155–5236.

4 D. J. Donaldson, A. F. Tuck and V. Vaida, *Chem. Rev.*, 2003, **103**, 4717–4730.

5 P. S. Monks, *Chem. Soc. Rev.*, 2005, **34**, 376–395.

6 B. J. Finlayson-Pitts and J. N. Pitts Jr, *Chemistry of the Upper and Lower Atmosphere: Theory, Experiments, and Applications*, Academic Press, San Diego, 1999.

7 P. S. Monks, A. T. Archibald, A. Colette, O. Cooper, M. Coyle, R. Derwent, D. Fowler, C. Granier, K. S. Law, G. E. Mills, D. S. Stevenson, O. Tarasova, V. Thouret, E. von Schneidemesser, R. Sommariva, O. Wild and M. L. Williams, *Atmos. Chem. Phys.*, 2015, **15**, 8889–8973.

8 C. George, M. Ammann, B. D'Anna, D. J. Donaldson and S. A. Nizkorodov, *Chem. Rev.*, 2015, **115**, 4218–4258.

9 M. E. Monge, T. Rosenorn, O. Favez, M. Muller, G. Adler, A. Abo Riziq, Y. Rudich, H. Herrmann, C. George and B. D'Anna, *Proc. Natl. Acad. Sci. U. S. A.*, 2012, **109**, 6840–6844.

10 J. L. Jimenez, M. R. Canagaratna, N. M. Donahue, A. S. H. Prevot, Q. Zhang, J. H. Kroll, P. F. DeCarlo, J. D. Allan, H. Coe, N. L. Ng, A. C. Aiken, K. S. Docherty, I. M. Ulbrich, A. P. Grieshop, A. L. Robinson, J. Duplissy, J. D. Smith, K. R. Wilson, V. A. Lanz, C. Hueglin, Y. L. Sun, J. Tian, A. Laaksonen, T. Raatikainen, J. Rautiainen, P. Vaattovaara, M. Ehn, M. Kulmala, J. M. Tomlinson, D. R. Collins, M. J. Cubison, E. J. Dunlea, J. A. Huffman, T. B. Onasch, M. R. Alfarra, P. I. Williams, K. Bower, Y. Kondo, J. Schneider, F. Drewnick, S. Borrmann, S. Weimer, K. Demerjian, D. Salcedo, L. Cottrell, R. Griffin, A. Takami, T. Miyoshi, S. Hatakeyama, A. Shimono, J. Y. Sun, Y. M. Zhang,

 © 2022 The Author(s). Published by the Royal Society of Chemistry

Open Access Article. Published on 13 de gener 2022. Downloaded on 2/2/2026 23:46:41.
This article is licensed under a Creative Commons Attribution 3.0 Unported Licence.

K. Dzepina, J. R. Kimmel, D. Sueper, J. T. Jayne, S. C. Herndon, A. M. Trimborn, L. R. Williams, E. C. Wood, A. M. Middlebrook, C. E. Kolb, U. Baltensperger and D. R. Worsnop, *Science*, 2009, **326**, 1525–1529.

11 M. Gen, R. Zhang, D. D. Huang, Y. Li and C. K. Chan, *Environ. Sci. Technol.*, 2019, **53**, 8757–8766.

12 M. Gen, R. Zhang, D. D. Huang, Y. Li and C. K. Chan, *Environ. Sci. Technol. Lett.*, 2019, **6**, 86–91.

13 H. Zheng, S. Song, G. Sarwar, M. Gen, S. Wang, D. Ding, X. Chang, S. Zhang, J. Xing, Y. Sun, D. Ji, C. K. Chan, J. Gao and M. B. McElroy, *Environ. Sci. Technol. Lett.*, 2020, **7**, 632–638.

14 H. Chen, C. E. Nanayakkara and V. H. Grassian, *Chem. Rev.*, 2012, **112**, 5919–5948.

15 M. Tang, D. J. Cziczo and V. H. Grassian, *Chem. Rev.*, 2016, **116**, 4205–4259.

16 B. C. Faust and R. G. Zepp, *Environ. Sci. Technol.*, 1993, **27**, 2517–2522.

17 C. Weller, A. Tilgner, P. Bräuer and H. Herrmann, *Environ. Sci. Technol.*, 2014, **48**, 5652–5659.

18 J. Mack and J. R. Bolton, *J. Photochem. Photobiol., A*, 1999, **128**, 1–13.

19 S. Goldstein and J. Rabani, *J. Am. Chem. Soc.*, 2007, **129**, 10597–10601.

20 R. Zellner, M. Exner and H. Herrmann, *J. Atmos. Chem.*, 1990, **10**, 411–425.

21 D. M. Bulman, S. P. Mezyk and C. K. Remucal, *Environ. Sci. Technol.*, 2019, **53**, 4450–4459.

22 S. Gligorovski and J. P. D. Abbatt, *Science*, 2018, **359**, 632–633.

23 J. X. Warner, R. R. Dickerson, Z. Wei, L. L. Strow, Y. Wang and Q. Liang, *Geophys. Res. Lett.*, 2017, **44**, 2875–2884.

24 C. Li, C. McLinden, V. Fioletov, N. Krotkov, S. Carn, J. Joiner, D. Streets, H. He, X. Ren, Z. Li and R. R. Dickerson, *Sci. Rep.*, 2017, **7**, 14304.

25 J. L. Hand, B. A. Schichtel, W. C. Malm and M. L. Pitchford, *Atmos. Chem. Phys.*, 2012, **12**, 10353–10365.

26 A. Franchin, D. L. Fibiger, L. Goldberger, E. E. McDuffie, A. Moravek, C. C. Womack, E. T. Crosman, K. S. Docherty, W. P. Dube, S. W. Hoch, B. H. Lee, R. Long, J. G. Murphy, J. A. Thornton, S. S. Brown, M. Baasandorj and A. M. Middlebrook, *Atmos. Chem. Phys.*, 2018, **18**, 17259–17276.

27 J.-P. Putaud, F. Raes, R. Van Dingenen, E. Brüggemann, M.-C. Facchini, S. Decesari, S. Fuzzi, R. Gehrig, C. Hüglin, P. Laj, G. Lorbeer, W. Maenhaut, N. Mihalopoulos, K. Müller, X. Querol, S. Rodriguez, J. Schneider, G. Spindler, H. ten Brink, K. Tørseth and A. Wiedensohler, *Atmos. Environ.*, 2004, **38**, 2579–2595.

28 G. Spindler, K. Müller, E. Brüggemann, T. Gnauk and H. Herrmann, *Atmos. Environ.*, 2004, **38**, 5333–5347.

29 I. Uno, Z. Wang, S. Itahashi, K. Yumimoto, Y. Yamamura, A. Yoshino, A. Takami, M. Hayasaki and B.-G. Kim, *Sci. Rep.*, 2020, **10**, 6450.

30 Y.-J. Jo, H.-J. Lee, H.-Y. Jo, J.-H. Woo, Y. Kim, T. Lee, G. Heo, S.-M. Park, D. Jung, J. Park and C.-H. Kim, *Atmos. Res.*, 2020, **240**, 104948.

31 Q. Xu, S. Wang, J. Jiang, N. Bhattarai, X. Li, X. Chang, X. Qiu, M. Zheng, Y. Hua and J. Hao, *Sci. Total Environ.*, 2019, **689**, 1293–1303.

32 X. Fu, T. Wang, J. Gao, P. Wang, Y. Liu, S. Wang, B. Zhao and L. Xue, *Environ. Sci. Technol.*, 2020, **54**, 3881–3889.

33 G. Mark, H. G. Korth, H. P. Schuchmann and C. Von Sonntag, *J. Photochem. Photobiol., A*, 1996, **101**, 89–103.

34 P. Kasibhatla, T. Sherwen, M. J. Evans, L. J. Carpenter, C. Reed, B. Alexander, Q. Chen, M. P. Sulprizio, J. D. Lee, K. A. Read, W. Bloss, L. R. Crilley, W. C. Keene, A. A. P. Pszenny and A. Hodzic, *Atmos. Chem. Phys.*, 2018, **18**, 11185–11203.

35 Y. Wu, L. Bu, X. Duan, S. Zhu, M. Kong, N. Zhu and S. Zhou, *J. Clean. Prod.*, 2020, **273**, 123065.

36 R. G. Zepp, J. Holgne and H. Bader, *Environ. Sci. Technol.*, 1987, **21**, 443–450.

37 R. Zhang, M. Gen, D. Huang, Y. Li and C. K. Chan, *Environ. Sci. Technol.*, 2020, **54**, 3831–3839.

38 C. Ye, N. Zhang, H. Gao and X. Zhou, *Environ. Sci. Technol.*, 2017, **51**, 6849–6856.

39 Q. Shi, Y. Tao, J. E. Krechmer, C. L. Heald, J. G. Murphy, J. H. Kroll and Q. Ye, *Environ. Sci. Technol.*, 2021, **55**, 854–861.

40 C. Ye, X. Zhou, D. Pu, J. Stutz, J. Festa, M. Spolaor, C. Tsai, C. Cantrell, R. L. Mauldin, T. Campos, A. Weinheimer, R. S. Hornbrook, E. C. Apel, A. Guenther, L. Kaser, B. Yuan, T. Karl, J. Haggerty, S. Hall, K. Ullmann, J. N. Smith, J. Ortega and C. Knote, *Nature*, 2016, **532**, 489–491.

41 P. Nissenson, D. Dabdub, R. Das, V. Maurino, C. Minero and D. Vione, *Atmos. Environ.*, 2010, **44**, 4859–4866.

42 N. K. Scharko, A. E. Berke and J. D. Raff, *Environ. Sci. Technol.*, 2014, **48**, 11991–12001.

43 L. M. Wingen, A. C. Moskun, S. N. Johnson, J. L. Thomas, M. Roeselová, D. J. Tobias, M. T. Kleinman and B. J. Finlayson-Pitts, *Phys. Chem. Chem. Phys.*, 2008, **10**, 5668–5677.

44 S. S. Brown and J. Stutz, *Chem. Soc. Rev.*, 2012, **41**, 6405–6447.

45 A. E. Perring, S. E. Pusede and R. C. Cohen, *Chem. Rev.*, 2013, **113**, 5848–5870.

46 J.-F. Müller, J. Peeters and T. Stavrakou, *Atmos. Chem. Phys.*, 2014, **14**, 2497–2508.

47 T. Nah, J. Sanchez, C. M. Boyd and N. L. Ng, *Environ. Sci. Technol.*, 2016, **50**, 222–231.

48 M. Daniels, R. V. Meyers and E. V. Belardo, *J. Phys. Chem.*, 1968, **72**, 389–399.

49 A. M. Grannas, A. E. Jones, J. Dibb, M. Ammann, C. Anastasio, H. J. Beine, M. Bergin, J. Bottenheim, C. S. Boxe, G. Carver, G. Chen, J. H. Crawford, F. Dominé, M. M. Frey, M. I. Guzmán, D. E. Heard, D. Helmig, M. R. Hoffmann, R. E. Honrath, L. G. Huey, M. Hutterli, H. W. Jacobi, P. Klán, B. Lefer, J. McConnell, J. Plane, R. Sander, J. Savarino, P. B. Shepson, W. R. Simpson,

Open Access Article. Published on 13 de gener 2022. Downloaded on 2/2/2026 23:46:41.
This article is licensed under a Creative Commons Attribution 3.0 Unported Licence.

J. R. Sodeau, R. Von Glasow, R. Weller, E. W. Wolff and T. Zhu, *Atmos. Chem. Phys.*, 2007, **7**, 4329–4373.
50 K. B. Benedict, A. S. McFall and C. Anastasio, *Environ. Sci. Technol.*, 2017, **51**, 4387–4395.
51 P. Warneck and C. Wurzinger, *J. Phys. Chem.*, 1988, **92**, 6278–6283.
52 T. Arakaki, C. Anastasio, Y. Kuroki, H. Nakajima, K. Okada, Y. Kotani, D. Handa, S. Azechi, T. Kimura, A. Tsuhako and Y. Miyagi, *Environ. Sci. Technol.*, 2013, **47**, 8196–8203.
53 G. Chen, S. Hanukovich, M. Chebeir, P. Christopher and H. Liu, *Environ. Sci. Technol.*, 2019, **53**, 316–324.
54 B. H. J. Bielski, D. E. Cabelli, R. L. Arudi and A. B. Ross, *J. Phys. Chem. Ref. Data*, 1985, **14**, 1041–1100.
55 S. Goldstein and G. Czapski, *Free Radic. Biol. Med.*, 1995, **19**, 505–510.
56 S. V Lymar and J. K. Hurst, *J. Am. Chem. Soc.*, 1995, **117**, 8867–8868.
57 O. Svoboda, L. Kubelová and P. Slavíček, *J. Phys. Chem. A*, 2013, **117**, 12868–12877.
58 K. R. Wilson, A. M. Prophet, G. Rovelli, M. D. Willis, R. J. Rapf and M. I. Jacobs, *Chem. Sci.*, 2020, **11**, 8533–8545.
59 D. E. Otten, P. B. Petersen and R. J. Saykally, *Chem. Phys. Lett.*, 2007, **449**, 261–265.
60 M. A. Brown, B. Winter, M. Faubel and J. C. Hemminger, *J. Am. Chem. Soc.*, 2009, **131**, 8354–8355.
61 C. Jie, C. D. Vecitis, M. R. Hoffmann and A. J. Colussi, *J. Phys. Chem. B*, 2006, **110**, 25598–25602.
62 M. Xu, R. Spinney and H. C. Allen, *J. Phys. Chem. B*, 2009, **113**, 4102–4110.
63 C. Tian, S. J. Byrnes, H. L. Han and Y. R. Shen, *J. Phys. Chem. Lett.*, 2011, **2**, 1946–1949.
64 S. N. Wren and D. J. Donaldson, *Chem. Phys. Lett.*, 2012, **522**, 1–10.
65 L. M. Pegram and M. T. Record, *Proc. Natl. Acad. Sci. U. S. A.*, 2006, **103**, 14278–14281.
66 J. L. Thomas, M. Roeselová, L. X. Dang and D. J. Tobias, *J. Phys. Chem. A*, 2007, **111**, 3091–3098.
67 B. Minofar, R. Vácha, A. Wahab, S. Mahiuddin, W. Kunz and P. Jungwirth, *J. Phys. Chem. B*, 2006, **110**, 15939–15944.
68 H. O. T. Pye, A. Nenes, B. Alexander, A. P. Ault, M. C. Barth, S. L. Clegg, J. L. Collett, K. M. Fahey, C. J. Hennigan, H. Herrmann, M. Kanakidou, J. T. Kelly, I. T. Ku, V. Faye McNeill, N. Riemer, T. Schaefer, G. Shi, A. Tilgner, J. T. Walker, T. Wang, R. Weber, J. Xing, R. A. Zaveri and A. Zuend, *Atmos. Chem. Phys.*, 2020, **20**, 4809–4888.
69 Q. Zhang, J. L. Jimenez, D. R. Worsnop and M. Canagaratna, *Environ. Sci. Technol.*, 2007, **41**, 3213–3219.
70 S. Enami, M. R. Hoffmann and A. J. Colussi, *Proc. Natl. Acad. Sci. U. S. A.*, 2008, **105**, 7365–7369.
71 N. K. Richards and B. J. Finlayson-Pitts, *Environ. Sci. Technol.*, 2012, **46**, 10447–10454.
72 G. A. Poskrebyshev, P. Neta and R. E. Huie, *J. Phys. Chem. A*, 2002, **106**, 11488–11491.
73 C. Anastasio and C. Liang, *Environ. Sci. Technol.*, 2009, **43**, 1108–1114.
74 E. Riordan, N. Minogue, D. Healy, P. O'Driscoll and J. R. Sodeau, *J. Phys. Chem. A*, 2005, **109**, 779–786.
75 T. C. Vandenboer, C. J. Young, R. K. Talukdar, M. Z. Markovic, S. S. Brown, J. M. Roberts and J. G. Murphy, *Nat. Geosci.*, 2015, **8**, 55–60.
76 H. Su, Y. Cheng, R. Oswald, T. Behrendt, I. Trebs, F. X. Meixner, M. O. Andreae, P. Cheng, Y. Zhang and U. Pöschl, *Science*, 2011, **333**, 1616–1618.
77 J. Y. Park and Y. N. Lee, *J. Phys. Chem.*, 1988, **92**, 6294–6302.
78 C. K. Chan, R. C. Flagan and J. H. Seinfeld, *Atmos. Environ., Part A*, 1992, **26**, 1661–1673.
79 M. C. Yeung and C. K. Chan, *Aerosol Sci. Technol.*, 2010, **44**, 269–280.
80 M. Roca, J. Zahardis, J. Bone, M. El-Maazawi and V. H. Grassian, *J. Phys. Chem. A*, 2008, **112**, 13275–13281.
81 P. K. Hudson, J. Schwarz, J. Baltrusaitis, E. R. Gibson and V. H. Grassian, *J. Phys. Chem. A*, 2007, **111**, 544–548.
82 S. A. Asher, D. D. Tuschel, T. A. Vargson, L. Wang and S. J. Geib, *J. Phys. Chem. A*, 2011, **115**, 4279–4287.
83 N. K. Richards-Henderson, C. Anderson, C. Anastasio and B. J. Finlayson-Pitts, *Phys. Chem. Chem. Phys.*, 2015, **17**, 32211–32218.
84 W. Yang, C. Han, H. Yang and X. Xue, *Environ. Pollut.*, 2018, **243**, 679–686.
85 S. Romakkaniemi, K. Hämeri, M. Väkevä and A. Laaksonen, *J. Phys. Chem. A*, 2001, **105**, 8183–8188.
86 L. Chu and C. Anastasio, *J. Phys. Chem. A*, 2003, **107**, 9594–9602.
87 K. B. Benedict and C. Anastasio, *J. Phys. Chem. A*, 2017, **121**, 8474–8483.
88 A. S. McFall, K. C. Edwards and C. Anastasio, *Environ. Sci. Technol.*, 2018, **52**, 5710–5717.
89 Y. Dubowski, A. J. Colussi, C. Boxe and M. R. Hoffmann, *J. Phys. Chem. A*, 2002, **106**, 6967–6971.
90 M. Zatko, L. Geng, B. Alexander, E. Sofen and K. Klein, *Atmos. Chem. Phys.*, 2016, **16**, 2819–2842.
91 F. Dominé and P. B. Shepson, *Science*, 2002, **297**, 1506–1510.
92 G. Marcotte, P. Marchand, S. Pronovost, P. Ayotte, C. Laffon and P. Parent, *J. Phys. Chem. A*, 2015, **119**, 1996–2005.
93 C. S. Blaszczak-Boxe and A. Saiz-Lopez, *Atmos. Environ.*, 2018, **193**, 224–241.
94 F. Domine, J. Bock, D. Voisin and D. J. Donaldson, *J. Phys. Chem. A*, 2013, **117**, 4733–4749.
95 C. Meusinger, T. A. Berhanu, J. Erbland, J. Savarino and M. S. Johnson, *J. Chem. Phys.*, 2014, **140**, 244305.
96 S. N. Wren and D. J. Donaldson, *J. Phys. Chem. Lett.*, 2011, **2**, 1967–1971.
97 K. J. Morenz, Q. Shi, J. G. Murphy and D. J. Donaldson, *J. Phys. Chem. A*, 2016, **120**, 7902–7908.
98 C. L. Weagle, G. Snider, C. Li, A. Van Donkelaar, S. Philip, P. Bissonnette, J. Burke, J. Jackson, R. Latimer, E. Stone, I. Abboud, C. Akoshile, N. X. Anh, J. R. Brook, A. Cohen, J. Dong, M. D. Gibson, D. Griffith, K. B. He, B. N. Holben, R. Kahn, C. A. Keller, J. S. Kim, N. Lagrosas, P. Lestari, Y. L. Khian, Y. Liu, E. A. Marais, J. V. Martins, A. Misra, U. Muliane, R. Pratiwi, E. J. Quel, A. Salam, L. Segev, S. N. Tripathi, C. Wang, Q. Zhang, M. Brauer, Y. Rudich

© 2022 The Author(s). Published by the Royal Society of Chemistry

Open Access Article. Published on 13 de gener 2022. Downloaded on 2/2/2026 23:46:41.
This article is licensed under a Creative Commons Attribution 3.0 Unported Licence.

and R. V. Martin, *Environ. Sci. Technol.*, 2018, **52**, 11670–11681.
99 C. K. Chan, Z. Liang, J. Zheng, S. L. Clegg and P. Brimblecombe, *Aerosol Sci. Technol.*, 1997, **27**, 324–344.
100 N. K. Richards-Henderson, K. M. Callahan, P. Nissenson, N. Nishino, D. J. Tobias and B. J. Finlayson-Pitts, *Phys. Chem. Chem. Phys.*, 2013, **15**, 17636–17646.
101 N. K. Richards, L. M. Wingen, K. M. Callahan, N. Nishino, M. T. Kleinman, D. J. Tobias and B. J. Finlayson-Pitts, *J. Phys. Chem. A*, 2011, **115**, 5810–5821.
102 L. Piatkowski, Z. Zhang, E. H. G. Backus, H. J. Bakker and M. Bonn, *Nat. Commun.*, 2014, **5**, 4083.
103 P. Jungwirth and D. J. Tobias, *J. Phys. Chem. B*, 2001, **105**, 10468–10472.
104 S. Ghosal, J. C. Hemminger, H. Bluhm, B. S. Mun, E. L. D. Hebenstreit, G. Ketteler, D. F. Ogletree, F. G. Requejo and M. Salmeron, *Science*, 2005, **307**, 563–566.
105 D. C. Blanchard, *J. Geophys. Res. Ocean.*, 1985, **90**, 961–963.
106 W. R. Simpson, S. S. Brown, A. Saiz-Lopez, J. A. Thornton and R. Von Glasow, *Chem. Rev.*, 2015, **115**, 4035–4062.
107 X. Fu, T. Wang, S. Wang, L. Zhang, S. Cai, J. Xing and J. Hao, *Environ. Sci. Technol.*, 2018, **52**, 1644–1654.
108 H. W. Xiao, H. Y. Xiao, L. Luo, C. Y. Shen, A. M. Long, L. Chen, Z. H. Long and D. N. Li, *Atmos. Chem. Phys.*, 2017, **17**, 3199–3214.
109 B. Wang, Y. Chen, S. Zhou, H. Li, F. Wang and T. Yang, *Sci. Total Environ.*, 2019, **649**, 652–660.
110 H. W. Xiao, H. Y. Xiao, C. Y. Shen, Z. Y. Zhang and A. M. Long, *Atmosphere*, 2018, **9**, 298.
111 R. Kumar, A. Elizabeth and A. G. Gawane, *Aerosol Sci. Technol.*, 2006, **40**, 477–489.
112 R. Rengarajan, A. K. Sudheer and M. M. Sarin, *Atmos. Res.*, 2011, **102**, 420–431.
113 L. Zhao, L. Wang, J. Tan, J. Duan, X. Ma, C. Zhang, S. Ji, M. Qi, X. H. Lu, Y. Wang, Q. Wang and R. Xu, *Atmos. Environ.*, 2019, **206**, 119–131.
114 H. Wang, J. Ding, J. Xu, J. Wen, J. Han, K. Wang, G. Shi, Y. Feng, C. E. Ivey, Y. Wang, A. Nenes, Q. Zhao and A. G. Russell, *Sci. Total Environ.*, 2019, **646**, 564–572.
115 D. Atzei, P. Fermo, R. Vecchi, M. Fantauzzi, V. Comite, G. Valli, F. Cocco and A. Rossi, *Environ. Pollut.*, 2019, **246**, 294–302.
116 D. K. Deshmukh, M. K. Deb, Y. I. Tsai and S. L. Mkoma, *Aerosol Air Qual. Res.*, 2011, **11**, 696–708.
117 P. Pipalatkar, V. V. Khaparde, D. G. Gajghate and M. A. Bawase, *Aerosol Air Qual. Res.*, 2014, **14**, 1089–1099.
118 B. J. Finlayson-Pitts, *Chem. Rev.*, 2003, **103**, 4801–4822.
119 B. J. Finlayson-Pitts, *Anal. Chem.*, 2010, **82**, 770–776.
120 J. L. Moyers and R. A. Duce, *J. Geophys. Res.*, 1972, **77**, 5229–5238.
121 Y.-H. Zhang and C. K. Chan, *J. Phys. Chem. A*, 2000, **104**, 9191–9196.
122 P. D. Pedersen, K. V. Mikkelsen and M. S. Johnson, *Phys. Chem. Chem. Phys.*, 2020, **22**, 11678–11685.
123 C. Ye, N. Zhang, H. Gao and X. Zhou, *Sci. Rep.*, 2019, **9**, 4351.
124 C. George, R. S. Strekowski, J. Kleffmann, K. Stemmler and M. Ammann, *Faraday Discuss.*, 2005, **130**, 195–210.
125 J. Liu, S. Li, M. Mekic, H. Jiang, W. Zhou, G. Loisel, W. Song, X. Wang and S. Gligorovski, *Environ. Sci. Technol. Lett.*, 2019, **6**, 413–417.
126 C. Han, W. Yang, Q. Wu, H. Yang and X. Xue, *Environ. Sci. Technol.*, 2016, **50**, 5017–5023.
127 K. Stemmler, M. Ammann, C. Donders, J. Kleffmann and C. George, *Nature*, 2006, **440**, 195–198.
128 X. Wang, E. Z. Dalton, Z. C. Payne, S. Perrier, M. Riva, J. D. Raff and C. George, *Environ. Sci. Technol. Lett.*, 2021, **8**, 53–58.
129 Z. Liang, R. Zhang, M. Gen, Y. Chu and C. K. Chan, *J. Phys. Chem. A*, 2021, **125**, 3739–3747.
130 B. Mayer and S. Madronich, *Atmos. Chem. Phys.*, 2004, **4**, 2241–2250.
131 P. Nissenson, C. J. H. Knox, B. J. Finlayson-Pitts, L. F. Phillips and D. Dabdub, *Phys. Chem. Chem. Phys.*, 2006, **8**, 4700–4710.
132 C. K. Chan, R. C. Flagan and J. H. Seinfeld, *Appl. Opt.*, 1991, **30**, 459–467.
133 B. Mayer, M. Schröder, R. Preusker and L. Schüller, *Atmos. Chem. Phys.*, 2004, **4**, 1255–1263.
134 F. J. Dentener, G. R. Carmichael, Y. Zhang, J. Lelieveld and P. J. Crutzen, *J. Geophys. Res. Atmos.*, 1996, **101**, 22869–22889.
135 B. R. G. Mabato, Y. Lyu, Y. Ji, Y. J. Li, D. D. Huang, X. Li, T. Nah, C. H. Lam and C. K. Chan, *Atmos. Chem. Phys.*, 2022, **22**, 273–293.
136 J. Baltrusaitis, J. Schuttlefield, J. H. Jensen and V. H. Grassian, *Phys. Chem. Chem. Phys.*, 2007, **9**, 4970–4980.
137 G. Rubasinghege and V. H. Grassian, *J. Phys. Chem. A*, 2009, **113**, 7818–7825.
138 D. M. B. Lesko, E. M. Coddens, H. D. Swomley, R. M. Welch, J. Borgatta and J. G. Navea, *Phys. Chem. Chem. Phys.*, 2015, **17**, 20775–20785.
139 J. Du and L. Zhu, *Chem. Phys. Lett.*, 2011, **511**, 213–218.
140 C. Zhu, B. Xiang, L. Zhu and R. Cole, *Chem. Phys. Lett.*, 2008, **458**, 373–377.
141 C. R. Usher, A. E. Michel and V. H. Grassian, *Chem. Rev.*, 2003, **103**, 4883–4940.
142 A. Gankanda and V. H. Grassian, *J. Phys. Chem. C*, 2014, **118**, 29117–29125.
143 A. Gankanda and V. H. Grassian, *J. Phys. Chem. A*, 2013, **117**, 2205–2212.
144 J. J. Jankowski, D. J. Kieber, K. Mopper and P. J. Neale, *Photochem. Photobiol.*, 2004, **71**, 431–440.
145 F. Bao, M. Li, Y. Zhang, C. Chen and J. Zhao, *Environ. Sci. Technol.*, 2018, **52**, 6309–6316.
146 P. S. Romer, P. J. Wooldridge, J. D. Crounse, M. J. Kim, P. O. Wennberg, J. E. Dibb, E. Scheuer, D. R. Blake, S. Meinardi, A. L. Brosius, A. B. Thames, D. O. Miller, W. H. Brune, S. R. Hall, T. B. Ryerson and R. C. Cohen, *Environ. Sci. Technol.*, 2018, **52**, 13738–13746.
147 C. Ye, H. Gao, N. Zhang and X. Zhou, *Environ. Sci. Technol.*, 2016, **50**, 3530–3536.

© 2022 The Author(s). Published by the Royal Society of Chemistry

Open Access Article. Published on 13 de gener 2022. Downloaded on 2/2/2026 23:46:41.
This article is licensed under a Creative Commons Attribution 3.0 Unported Licence.

148 A. M. Baergen and D. J. Donaldson, *Environ. Sci. Technol.*, 2013, **47**, 815–820.
149 S. Laufs and J. Kleffmann, *Phys. Chem. Chem. Phys.*, 2016, **18**, 9616–9625.
150 M. N. Sullivan, L. T. Chu and L. Zhu, *Phys. Chem. Chem. Phys.*, 2018, **20**, 30537–30539.
151 R. Sander, *Atmos. Chem. Phys.*, 2015, **15**, 4399–4981.
152 T. C. Bond and R. W. Bergstrom, *Aerosol Sci. Technol.*, 2006, **40**, 27–67.
153 A. Laskin, J. Laskin and S. A. Nizkorodov, *Chem. Rev.*, 2015, **115**, 4335–4382.
154 M. Shiraiwa, Y. Kondo, N. Moteki, N. Takegawa, Y. Miyazaki and D. R. Blake, *Geophys. Res. Lett.*, 2007, **34**, L16803.
155 D. A. Lack, J. M. Langridge, R. Bahreini, C. D. Cappa, A. M. Middlebrook and J. P. Schwarz, *Proc. Natl. Acad. Sci. U. S. A.*, 2012, **109**, 14802–14807.
156 T. Moise, J. M. Flores and Y. Rudich, *Chem. Rev.*, 2015, **115**, 4400–4439.
157 R. F. Hems, E. G. Schnitzler, C. Liu-Kang, C. D. Cappa and J. P. D. Abbatt, *ACS Earth Space Chem.*, 2021, **5**, 722–748.
158 Y. Wang, D. D. Huang, W. Huang, B. Liu, Q. Chen, R. Huang, M. Gen, B. R. G. Mabato, C. K. Chan, X. Li, T. Hao, Y. Tan, K. I. Hoi, K. M. Mok and Y. J. Li, *Environ. Sci. Technol.*, 2021, **55**, 15694–15704.
159 M. Gen, R. Zhang and C. K. Chan, *Environ. Sci. Technol.*, 2021, **55**, 15715–15723.
160 A. Alif and P. Boule, *J. Photochem. Photobiol., A*, 1991, **59**, 357–367.
161 A. Bianco, M. Passananti, H. Perroux, G. Voyard, C. Mouchel-Vallon, N. Chaumerliac, G. Mailhot, L. Deguillaume and M. Brigante, *Atmos. Chem. Phys.*, 2015, **15**, 9191–9202.
162 H. Herrmann, *Chem. Rev.*, 2003, **103**, 4691–4716.
163 H. Herrmann, D. Hoffmann, T. Schaefer, P. Bräuer and A. Tilgner, *ChemPhysChem*, 2010, **11**, 3796–3822.
164 H. Herrmann, T. Schaefer, A. Tilgner, S. A. Styler, C. Weller, M. Teich and T. Otto, *Chem. Rev.*, 2015, **115**, 4259–4334.
165 B. Ervens, A. Sorooshian, Y. B. Lim and B. J. Turpin, *J. Geophys. Res.*, 2014, **119**, 3997–4016.
166 Y. Cheng, G. Zheng, C. Wei, Q. Mu, B. Zheng, Z. Wang, M. Gao, Q. Zhang, K. He, G. Carmichael, U. Pöschl and H. Su, *Sci. Adv.*, 2016, **2**, e1601530.
167 A. C. Hong, S. N. Wren and D. J. Donaldson, *J. Phys. Chem. Lett.*, 2013, **4**, 2994–2998.
168 B. Zheng, Q. Zhang, Y. Zhang, K. B. He, K. Wang, G. J. Zheng, F. K. Duan, Y. L. Ma and T. Kimoto, *Atmos. Chem. Phys.*, 2015, **15**, 2031–2049.
169 M. Kanakidou, J. H. Seinfeld, S. N. Pandis, I. Barnes, F. J. Dentener, M. C. Facchini, R. Van Dingenen, B. Ervens, A. Nenes, C. J. Nielsen, E. Swietlicki, J. P. Putaud, Y. Balkanski, S. Fuzzi, J. Horth, G. K. Moortgat, R. Winterhalter, C. E. L. Myhre, K. Tsigaridis, E. Vignati, E. G. Stephanou and J. Wilson, *Atmos. Chem. Phys.*, 2005, **5**, 1053–1123.
170 A. G. Carlton, B. J. Turpin, H. J. Lim, K. E. Altieri and S. Seitzinger, *Geophys. Res. Lett.*, 2006, **33**, L06822.
171 Y. Liu, I. El Haddad, M. Scarfogliero, L. Nieto-Gligorovski, B. Temime-Roussel, E. Quivet, N. Marchand, B. Picquet-Varrault and A. Monod, *Atmos. Chem. Phys.*, 2009, **9**, 5093–5105.
172 L. Poulain, Y. Katrib, E. Isikli, Y. Liu, H. Wortham, P. Mirabel, S. Le Calvé and A. Monod, *Chemosphere*, 2010, **81**, 312–320.
173 X. Zhang, Z. M. Chen and Y. Zhao, *Atmos. Chem. Phys.*, 2010, **10**, 9551–9561.
174 A. K. Y. Lee, P. Herckes, W. R. Leaitch, A. M. MacDonald and J. P. D. Abbatt, *Geophys. Res. Lett.*, 2011, **38**, L11805.
175 D. D. Huang, Q. Zhang, H. H. Y. Cheung, L. Yu, S. Zhou, C. Anastasio, J. D. Smith and C. K. Chan, *Environ. Sci. Technol.*, 2018, **52**, 9215–9224.
176 R. Zhang, M. Gen, T.-M. Fu and C. K. Chan, *Environ. Sci. Technol.*, 2021, **55**, 5711–5720.
177 B. R. G. Mabato, M. Gen, Y. Chu and C. K. Chan, *ACS Earth Space Chem.*, 2019, **3**, 150–157.
178 M. Gen, D. D. Huang and C. K. Chan, *Environ. Sci. Technol.*, 2018, **52**, 6903–6911.
179 R. Zhang, M. Gen, Z. Liang, Y. J. Li and C. K. Chan, *Environ. Sci. Technol.*, 2022, DOI: 10.1021/acs.est.1c07211.
180 M. Z. Jacobson, *J. Geophys. Res. Atmos.*, 1999, **104**, 3527–3542.
181 B. R. G. Mabato, Y. Lyu, Y. Ji, D. D. Huang, X. Li, T. Nah, C. H. Lam and C. K. Chan, *Atmos. Chem. Phys. Discuss.*, 2021, **2021**, 1–35.
182 J. Yang, W. C. Au, H. Law, C. H. Lam and T. Nah, *Atmos. Environ.*, 2021, **254**, 118401.
183 A. Kahnt, S. Behrouzi, R. Vermeylen, M. Safi Shalamzari, J. Vercauteren, E. Roekens, M. Claeys and W. Maenhaut, *Atmos. Environ.*, 2013, **81**, 561–568.
184 C. Mohr, F. D. Lopez-Hilfiker, P. Zotter, A. S. H. Prévoît, L. Xu, N. L. Ng, S. C. Herndon, L. R. Williams, J. P. Franklin, M. S. Zahniser, D. R. Worsnop, W. B. Knighton, A. C. Aiken, K. J. Gorkowski, M. K. Dubey, J. D. Allan and J. A. Thornton, *Environ. Sci. Technol.*, 2013, **47**, 6316–6324.
185 M. Teich, D. Van Pinxteren, M. Wang, S. Kecorius, Z. Wang, T. Müller, G. Močnik and H. Herrmann, *Atmos. Chem. Phys.*, 2017, **17**, 1653–1672.
186 F. Li, S. Tang, N. T. Tsona and L. Du, *Atmos. Environ.*, 2020, **237**, 117650.
187 Z. Kitanovski, A. Čusak, I. Grgić and M. Claeys, *Atmos. Meas. Tech.*, 2014, **7**, 2457–2470.
188 A. L. Klodt, D. E. Romonosky, P. Lin, J. Laskin, A. Laskin and S. A. Nizkorodov, *ACS Earth Space Chem.*, 2019, **3**, 2736–2746.
189 H. Pang, Q. Zhang, X. Lu, K. Li, H. Chen, J. Chen, X. Yang, Y. Ma, J. Ma and C. Huang, *Environ. Sci. Technol.*, 2019, **53**, 14253–14263.
190 G. Loisel, M. Mekic, S. Liu, W. Song, B. Jiang, Y. Wang, H. Deng and S. Gligorovski, *Atmos. Environ.*, 2021, **246**, 118140.
191 W. Walcher, T. Franze, M. G. Weller, U. Pöschl and C. G. Huber, *J. Proteome Res.*, 2003, **2**, 534–542.

© 2022 The Author(s). Published by the Royal Society of Chemistry

Open Access Article. Published on 13 de gener 2022. Downloaded on 2/2/2026 23:46:41.
This article is licensed under a Creative Commons Attribution 3.0 Unported Licence.

192 Y. K. Gruijthuijsen, I. Grieshuber, A. Stöcklinger, U. Tischler, T. Fehrenbach, M. G. Weller, L. Vogel, S. Vieths, U. Pöschl and A. Duschl, *Int. Arch. Allergy Immunol.*, 2006, **141**, 265–275.
193 Y. Zhang, H. Yang and U. Pöschl, *Anal. Bioanal. Chem.*, 2011, **399**, 459–471.
194 M. Shiraiwa, K. Selzle and U. Pöschl, *Free Radic. Res.*, 2012, **46**, 927–939.
195 M. Shiraiwa, K. Selzle, H. Yang, Y. Sosedova, M. Ammann and U. Pöschl, *Environ. Sci. Technol.*, 2012, **46**, 6672–6680.
196 A. Ghiani, M. Bruschi, S. Citterio, E. Bolzacchini, L. Ferrero, G. Sangiorgi, R. Asero and M. G. Perrone, *Sci. Total Environ.*, 2016, **573**, 1589–1597.
197 D. Vione, V. Maurino, C. Minero, E. Pelizzetti, M. A. J. Harrison, R. I. Olariu and C. Arsenec, *Chem. Soc. Rev.*, 2006, **35**, 441–453.
198 R. Niessen, D. Lenoir and P. Boule, *Chemosphere*, 1988, **17**, 1977–1984.
199 D. Guillaume, J. Morvan and G. Martin, *Environ. Technol. Lett.*, 1989, **10**, 491–500.
200 F. Machado and P. Boule, *J. Photochem. Photobiol., A*, 1995, **86**, 73–80.
201 D. Vione, V. Maurino, C. Minero, M. Lucchiari and E. Pelizzetti, *Chemosphere*, 2004, **56**, 1049–1059.
202 P. Lin, J. Liu, J. E. Shilling, S. M. Kathmann, J. Laskin and A. Laskin, *Phys. Chem. Chem. Phys.*, 2015, **17**, 23312–23325.
203 Z. Finewax, J. A. De Gouw and P. J. Ziemann, *Environ. Sci. Technol.*, 2018, **52**, 1981–1989.
204 J. L. Chang and J. E. Thompson, *Atmos. Environ.*, 2010, **44**, 541–551.
205 J. D. Smith, H. Kinney and C. Anastasio, *Atmos. Environ.*, 2016, **126**, 36–44.
206 P. Lin, N. Bluvshtein, Y. Rudich, S. A. Nizkorodov, J. Laskin and A. Laskin, *Environ. Sci. Technol.*, 2017, **51**, 11561–11570.
207 M. Xie, X. Chen, M. D. Hays and A. L. Holder, *Atmos. Chem. Phys.*, 2019, **19**, 2899–2915.
208 K. Vidović, A. Kroflič, M. Šala and I. Grgić, *Atmosphere*, 2020, **11**, 131.
209 S. Morville, A. Scheyer, P. Mirabel and M. Millet, *J. Environ. Monit.*, 2004, **6**, 963–966.
210 Y. Iinuma, O. Böge and H. Herrmann, *Environ. Sci. Technol.*, 2010, **44**, 8453–8459.
211 A. Roger, S. M. Aschmann and A. Janet, *Environ. Sci. Technol.*, 1992, **26**, 1397–1403.
212 M. A. J. Harrison, S. Barra, D. Borghesi, D. Vione, C. Arsene and R. Iulian Olariu, *Atmos. Environ.*, 2005, **39**, 231–248.
213 D. Vione, V. Maurino, C. Minero, M. Vincenti and E. Pelizzetti, *Chemosphere*, 2001, **44**, 237–248.
214 D. Vione, V. Maurino, C. Minero and E. Pelizzetti, *Chemosphere*, 2001, **45**, 893–902.
215 R. G. Coombes, A. W. Diggle and S. P. Kempsell, *Tetrahedron Lett.*, 1994, **35**, 6373–6376.
216 J. Dzengel, J. Theurich and D. W. Bahnemann, *Environ. Sci. Technol.*, 1999, **33**, 294–300.
217 J. J. Cole, E.-C. Lin, C. R. Barry and H. O. Jacobs, *Appl. Phys. Lett.*, 2009, **95**, 113101.
218 P. Warneck and C. Wurzinger, *J. Phys. Chem.*, 1988, **92**, 6278–6283.
219 M. Fischer and P. Warneck, *J. Phys. Chem.*, 1996, **100**, 18749–18756.
220 D. Vione, V. Maurino, C. Minero and E. Pelizzetti, *Environ. Sci. Technol.*, 2002, **36**, 669–676.
221 D. Vione, V. Maurino, C. Minero, D. Borghesi, M. Lucchiari and E. Pelizzetti, *Environ. Sci. Technol.*, 2003, **37**, 4635–4641.
222 D. Vione, V. Maurino, C. Minero and E. Pelizzetti, *Environ. Sci. Technol.*, 2005, **39**, 1101–1110.
223 D. Borghesi, D. Vione, V. Maurino and C. Minero, *J. Atmos. Chem.*, 2005, **52**, 259–281.
224 R. Arimoto, W. Balsam and C. Schloesslin, *Atmos. Environ.*, 2002, **36**, 89–96.
225 C. Minero, F. Bono, F. Rubertelli, D. Pavino, V. Maurino, E. Pelizzetti and D. Vione, *Chemosphere*, 2007, **66**, 650–656.
226 Y. Wang, M. Mekic, P. Li, H. Deng, S. Liu, B. Jiang, B. Jin, D. Vione and S. Gligorovski, *Environ. Sci. Technol.*, 2021, **55**, 4553–4564.
227 C. Reed, M. J. Evans, L. R. Crilley, W. J. Bloss, T. Sherwen, K. A. Read, J. D. Lee and L. J. Carpenter, *Atmos. Chem. Phys.*, 2017, **17**, 4081–4092.

© 2022 The Author(s). Published by the Royal Society of Chemistry